University of Nebraska - Lincoln
DigitalCommons@University of Nebraska - Lincoln

Faculty Papers and Publications in Animal Science | Animal Science Department

2017

Early transcriptome responses of the bovine midcycle corpus luteum to prostaglandin F2α includes cytokine signaling

Heather Talbott
University of Nebraska Medical Center, heather.talbott@unmc.edu

Xiaoying Artegoitia
University of Nebraska Medical Center, xhou@unmc.edu

Fang Qiu
University of Nebraska Medical Center, fqiu@unmc.edu

Pan Zhang
University of Nebraska Medical Center, pan.zhang@unmc.edu

Chittibabu Guda
University of Nebraska Medical Center, babu.guda@unmc.edu

See next page for additional authors

Follow this and additional works at: http://digitalcommons.unl.edu/animalscifacpub

 Part of the Genetics and Genomics Commons, and the Meat Science Commons

Talbott, Heather; Artegoitia, Xiaoying; Qiu, Fang; Zhang, Pan; Guda, Chittibabu; Yu, Fang; Cushman, Robert A.; Wood, Jennifer R.; Wang, Cheng; Cupp, Andrea S.; and Davis, John S., "Early transcriptome responses of the bovine midcycle corpus luteum to prostaglandin F2α includes cytokine signaling" (2017). *Faculty Papers and Publications in Animal Science*. 982.
http://digitalcommons.unl.edu/animalscifacpub/982

This Article is brought to you for free and open access by the Animal Science Department at DigitalCommons@University of Nebraska - Lincoln. It has been accepted for inclusion in Faculty Papers and Publications in Animal Science by an authorized administrator of DigitalCommons@University of Nebraska - Lincoln.

Authors
Heather Talbott, Xiaoying Artegoitia, Fang Qiu, Pan Zhang, Chittibabu Guda, Fang Yu, Robert A. Cushman, Jennifer R. Wood, Cheng Wang, Andrea S. Cupp, and John S. Davis

This article is available at DigitalCommons@University of Nebraska - Lincoln: http://digitalcommons.unl.edu/animalscifacpub/982

Molecular and Cellular Endocrinology 452 (2017) 93–109

Contents lists available at ScienceDirect

Molecular and Cellular Endocrinology

journal homepage: www.elsevier.com/locate/mce

Early transcriptome responses of the bovine midcycle corpus luteum to prostaglandin F2α includes cytokine signaling

Heather Talbott [a, b], Xiaoying Hou [a], Fang Qiu [c], Pan Zhang [a], Chittibabu Guda [d], Fang Yu [c], Robert A. Cushman [e], Jennifer R. Wood [f], Cheng Wang [a], Andrea S. Cupp [f], John S. Davis [a, b, g, *]

[a] Olson Center for Women's Health/Obstetrics and Gynecology Department, University of Nebraska Medical Center, 989450 Nebraska Medical Center, Omaha, NE 68198-9450, USA
[b] Biochemistry and Molecular Biology Department, University of Nebraska Medical Center, 985870 Nebraska Medical Center, Omaha, NE 68198-5870, USA
[c] Biostatistics Department, University of Nebraska Medical Center, 984375 Nebraska Medical Center, Omaha, NE 68198-4375, USA
[d] Department of Genetics, Cell Biology and Anatomy, Bioinformatics and Systems Biology Core, University of Nebraska Medical Center, 985805 Nebraska Medical Center, Omaha, NE 68198-5805, USA
[e] Nutrition and Environmental Management Research Unit, United States Department of Agriculture, P.O. Box 166 (State Spur 18D)/USDA-ARS-PA-USMARC, Clay Center, NE 68933, USA
[f] Animal Science Department, University of Nebraska—Lincoln, P.O. Box 830908, C203 ANSC, Lincoln, NE 68583-0908, USA
[g] Veterans Affairs Medical Center, 4101 Woolworth Ave, Omaha, NE 68105, USA

ARTICLE INFO

Article history:
Received 13 March 2017
Received in revised form
17 May 2017
Accepted 18 May 2017
Available online 23 May 2017

Keywords:
Corpus luteum
PGF2α
Regression
Cytokine
Signaling
Luteolysis

ABSTRACT

In ruminants, prostaglandin F2alpha (PGF2α)-mediated luteolysis is essential prior to estrous cycle resumption, and is a target for improving fertility. To deduce early PGF2α-provoked changes in the corpus luteum a short time-course (0.5–4 h) was performed on cows at midcycle. A microarray-determined transcriptome was established and examined by bioinformatic pathway analysis. Classic PGF2α effects were evident by changes in early response genes (FOS, JUN, ATF3) and prediction of active pathways (PKC, MAPK). Several cytokine transcripts were elevated and NF-κB and STAT activation were predicted by pathway analysis. Self-organizing map analysis grouped differentially expressed transcripts into ten mRNA expression patterns indicative of temporal signaling cascades. Comparison with two analogous datasets revealed a conserved group of 124 transcripts similarly altered by PGF2α treatment, which both, directly and indirectly, indicated cytokine activation. Elevated levels of cytokine transcripts after PGF2α and predicted activation of cytokine pathways implicate inflammatory reactions early in PGF2α-mediated luteolysis.

Published by Elsevier Ireland Ltd.

1. Introduction

In mammals, multiple fertile cycles depend on the formation and regression of a transient endocrine structure in the ovary termed the corpus luteum (CL) (Meidan, 2017). The CL forms during each estrous cycle and synthesizes progesterone, a hormone critical for early embryonic survival during pregnancy (Micks et al., 2015; Spencer et al., 2016). However, before the next follicle can develop, the steroidogenic luteal cells of the CL must cease progesterone production—contingent on the absence of a pregnancy—and ultimately undergo apoptosis (Aboelenain et al., 2015; Del Canto et al., 2007). Prostaglandin F2alpha (PGF2α) is a recognized lipid mediator that triggers luteal regression after an unsuccessful reproductive cycle or at parturition in mammals (Davis and Rueda, 2002). Thus, PGF2α-mediated luteolysis is a key checkpoint in the reproductive cycle and is a useful target for controlling the estrous cycle and fertility.

Signaling by PGF2α has been studied extensively *in vitro*, and the classic signaling pathway involves the binding of PGF2α to its G-protein coupled receptor and activating $G\alpha_{q/11}$ (McCann and Flint,

* Corresponding author. Olson Center for Women's Health, University of Nebraska Medical Center, 983255 Nebraska Medical Center, Omaha, NE 68198-3255, USA.
E-mail addresses: heather.talbott@unmc.edu (H. Talbott), xhou@unmc.edu (X. Hou), fqiu@unmc.edu (F. Qiu), pan.zhang@unmc.edu (P. Zhang), babu.guda@unmc.edu (C. Guda), fangyu@unmc.edu (F. Yu), bob.cushman@ars.usda.gov (R.A. Cushman), jwood5@unl.edu (J.R. Wood), chengwang@unmc.edu (C. Wang), acupp2@unl.edu (A.S. Cupp), jsdavis@unmc.edu (J.S. Davis).

http://dx.doi.org/10.1016/j.mce.2017.05.018
0303-7207/Published by Elsevier Ireland Ltd.

This document is a U.S. government work and is not subject to copyright in the United States.

Abbreviations

Protein/*Gene*
ABCA1 ATP binding cassette subfamily A member 1
ABCG1 ATP binding cassette subfamily G member 1
APOA1 apolipoprotein A1
APOE apolipoprotein E
ATF3/*ATF3* activating transcription factor 3
CCL/*CCL* C-C motif chemokine
CH25H/*CH25H* cholesterol 25-hydroxylase
CL corpus luteum
CYP11A1 cytochrome P450 family 11 subfamily A member 1
EDN1 endothelin 1
EGR/*EGR* early growth response protein 1/3/4
ERK extracellular signal-regulated kinase
FOS/*FOS* Finkel-Biskis-Jinkins murine osteosarcoma viral oncogene homolog
GEO Gene Expression Omnibus
HEPES 4-(2-hydroxyethyl)-1-piperazineethanesulfonic acid
HSD3B1 hydroxyl-δ-5-steroid dehydrogenase, 3 β and steroid δ-isomerase 1
HSL/*LIPE* Hormone sensitive lipase, type E
IL-/*IL* interleukin
INSIG1/*INSIG1* insulin induced gene 1
IPA Ingenuity Pathway Analysis
JUN/*JUN* Jun proto-oncogene
LDLR low density lipoprotein receptor
LDLRAP1/*LDLRAP1* low density lipoprotein receptor adaptor protein 1
LHCGR Luteinizing hormone/chorionic gonadotropin receptor
LLC large luteal cells
MAPK mitogen-activated protein kinase
mRNA messenger RNA
NF-κB/*NFKB1* nuclear factor kappa B
NR1H nuclear receptor family 1 subfamily H member 2/3
NR4A/*NR4A* nuclear receptor subfamily 4 group A member 1/2/3
PGF2α prostaglandin F2alpha
PKC/*PKCD* protein kinase C
qPCR quantitative real-time PCR
RMA robust multi-array average
SCARB1 scavenger receptor class B member 1
SEM standard error of the mean
SLC small luteal cells
SOM self-organizing map
StAR/*StAR* steroidogenic acute regulatory protein
STAT signal transducer and activator of transcription 1/3
TGFβ/*TGFB* transforming growth factor beta 1/2
TNFα/*TNF* tumor necrosis factor alpha
USF1 upstream transcription factor 1
VEGF vascular endothelial growth factor A

1993; Väänänen et al., 1998). The early intracellular signaling events initiated by PGF2α in luteal cells include the activation of phospholipase C (Davis et al., 1987), phospholipase A2 (Kurusu et al., 2012, 1998), an increase in intracellular Ca^{2+} (Davis et al., 1987), activation of protein kinase C (PKC) (Chen et al., 2001) and activation of mitogen-activated protein kinase (MAPK) signaling cascades including extracellular signal-regulated kinase (ERK) (Arvisais et al., 2010; Chen et al., 2001, 1998; Yadav and Medhamurthy, 2006). These signaling cascades are responsible for the induction of several early response genes including, Finkel-Biskis-Jinkins murine osteosarcoma viral oncogene homolog (*FOS*) (Chen et al., 2001), Jun proto-oncogene (*JUN*) (Chen et al., 2001), early growth response 1 (*EGR1*) (Hou et al., 2008), and activating transcription factor 3 (*ATF3*) (Mao et al., 2013). These initial alterations will trigger changes in the CL proteome enabling luteolysis to proceed. For example, EGR1 expression stimulates the synthesis of transforming growth factor beta (TGFβ) (Hou et al., 2008), which can inhibit luteal progesterone secretion (Hou et al., 2008), act on luteal endothelial cells to disrupt the microvasculature (Maroni and Davis, 2011), and stimulate the profibrotic activity of luteal fibroblasts (Maroni and Davis, 2012).

The luteolytic process is a well-coordinated series of events similar to an acute inflammatory response consisting of a sequential time-dependent infiltration of neutrophils, macrophages, and T lymphocytes (Best et al., 1996; Penny et al., 1999). Accordingly, there is likely time-dependent secretion of cytokines to recruit and activate the various leukocytes (Townson and Liptak, 2003). Several cytokine transcripts are induced by PGF2α in the mid-to late-stage CL including tumor necrosis factor alpha (*TNF*) (Shah et al., 2014), interleukin 1 beta (*IL1B*) (Atli et al., 2012; Mondal et al., 2011), *TGFB1* (Hou et al., 2008; Mondal et al., 2011; Shah et al., 2014), and the chemokines; C-C motif chemokine ligand 2 (*CCL2*, previously known as *MCP1*) (Mondal et al., 2011; Penny et al., 1998) and C-X-C motif 8 (*CXCL8*, previously known as *IL8*) (Atli et al., 2012; Mondal et al., 2011; Shah et al., 2014; Shirasuna et al., 2012b; Talbott et al., 2014). These cytokines have pleiotropic effects on luteal cells, including inhibition of progesterone secretion, stimulation of PGF2α secretion, and stimulation of apoptosis of multiple luteal cell types (Pate et al., 2010). The production of luteolytic factors, decrease in progesterone secretion, recruitment of immune cells, release of pro-inflammatory cytokines, reduction in blood supply (Shirasuna, 2010), and the creation of a hypoxic environment (Nishimura and Okuda, 2015) likely act in concert within the CL to cause the functional and structural regression of the CL.

The purpose of this study was to understand the early PGF2α-elicited changes in the CL based on temporal patterns of early transcript expression following *in vivo* treatment with PGF2α. While many studies have examined luteolytic alterations both *in vivo* and *in vitro*, most studies have focused on changes 3–24 h after PGF2α administration (Mondal et al., 2011; Shah et al., 2014) or used targeted rather than global approaches (Atli et al., 2012; Shirasuna et al., 2012a, 2010). Therefore, little is known about the very early temporal changes in global mRNA expression elicited in response to PGF2α treatment *in vivo*. In the present study, a systems biology approach using Affymetrix Bovine microarray was employed to evaluate gene expression at 0.5–4 h after PGF2α; followed by bioinformatics analysis of PGF2α-mediated signals. We hypothesized that the sequence of events after *in vivo* PGF2α administration would include early changes of classical targets of PGF2α signaling pathways followed by fluctuations in targets of cytokine signaling at later times.

2. Materials and methods

2.1. Animals

Postpubertal multiparous female cattle (n = 15) of composite breeding (½ Red Angus, Pinzgauer, Red Poll, Hereford and ½ Red

Angus and Gelbvieh) were synchronized using two intramuscular injections of PGF2α (25 mg; Lutalyse®, Zoetis Inc., Kalamazoo Michigan, MI) 11 days apart. At midcycle (days 9–10), cows were treated with an intra-muscular injection of saline (n = 3) or PGF2α (n = 12). At each of four times post-injection (0.5, 1, 2, and 4 h) three cows per treatment were subjected to a bilateral ovariectomy through a right flank approach under local anesthesia (Summers et al., 2014; Youngquist et al., 1995). The CL was dissected from the ovary, weighed and < 5 mm^3 sections were snap-frozen in liquid N_2 for subsequent protein and RNA analysis. Plasma progesterone concentrations were determined using the ImmuChem Progesterone DA Coated Tube radioimmunoassay kit (MP Biomedicals, Santa Ana, CA) with an intra-assay coefficient of variation of 9.13% and inter-assay coefficient of variation of 7.99%. The University of Nebraska-Lincoln Institutional Animal Care and Use Committee approved all procedures and facilities used in this animal experiment. Statistical differences in animal characteristics were determined using Kruskal-Wallis test followed by Dunn's post-test or one-way ANOVA followed by Bonferroni's multiple comparison test as appropriate (GraphPad Prism, La Jolla, CA).

2.2. Steroidogenic luteal cell culture

Bovine ovaries were collected during midcycle or early pregnancy from a local slaughterhouse (JBS® USA, Omaha, NE). Steroidogenic cells were prepared from luteal slices by enzymatic digestion with type II collagenase (103 IU/mL) as described previously (Hou et al., 2008). Enriched fractions of small luteal cells (SLC) and large luteal cells (LLC) were prepared from corpora lutea of early pregnancy using centrifugal elutriation similar to a previous study (Mao et al., 2013). The mixed luteal cells were resuspended in elutriation medium (calcium-free Dulbecco's modified eagle medium (DMEM) [D9800-10 US Biological, Salem, MA], supplemented with 25 mM 4-(2-hydroxyethyl)-1-piperazineethanesulfonic acid (HEPES), 3.89 g/L sodium bicarbonate, and 3 mg/mL glucose). Resuspended mixed luteal cells were subjected to centrifugal elutriation with continuous flow using a Beckman Coulter Avanti J-20 XP centrifuge equipped with a Beckman JE-5.0 elutriator rotor. After removing red blood cells and endothelial cells fractions containing primarily SLC (1200 rpm, 24 mL/min) and LLC (680 rpm, 30 mL/min) were collected. The SLC and LLC fractions were pelleted and resuspended in basal M199 (0.1% bovine serum albumin (BSA), 100 U/ml penicillin, 100 μg/mL streptomycin, and 10 μg/mL gentamycin). The average purity of SLC was ~ 90% and LLC was > 50%.

Cells were seeded at a density of 1×10^5 cells/cm^2 for midcycle mixed luteal cells and SLC and a density of 4×10^4 cells/cm^2 for LLC. Cells were allowed to attach in a 5% CO_2 incubator at 37 °C in basal M199 medium containing 5% fetal bovine serum (FBS). The cells were incubated in serum-free medium for 3 h before applying treatments as described in the legends to the figures [PGF2α (in ethanol, #16010, Cayman Chemical, Ann Arbor, MI), TNFα (210-TA, R&D, Minneapolis, MN), IL-1β (RP0106B), IL-6 (RP0014B), IL-17A (RP0056B, Kingfisher Biotech, Saint Paul, MN)]. Luteal cell cultures were harvested into lysis buffer (20 mM Tris [pH 7.5], 150 mM NaCl, 1 mM EDTA, 0.2 mM EGTA, 1% Triton X-100, protease and phosphatase inhibitor cocktails) and lysed by sonication.

Lysate supernatents were suspended in sodium dodecyl sulfate (SDS) loading buffer (50 mM Tris [pH 6.8], 300 mM glycerol, 25 mM SDS, 45 mM dithiothreitol, 260 mM 2-mercaptoethanol, bromophenol blue). Proteins were separated by electrophoresis using 10% SDS-polyacrylamide gels and transferred to nitrocellulose membranes. Membranes were blocked with 5% non-fat milk in 0.1% Tween 20 in Tris-buffered saline (TBST) and primary and secondary antibodies were diluted in 1% non-fat milk or BSA in 0.1% TBST. Signals were visualized on FluorChem M (ProteinSimple, San Jose, CA) or UVP (UVP, LLC, Upland, CA) systems using SuperSignal West Femto (Thermo Science, Miami, OK) or Western Lightening (PerkinElmer, Waltham, MA). Phosphorylated nuclear factor kappa B (NF-κB) subunit P65 (phospho-P65, 3031 AB_330559) and phosphorylated ERK1/2 P44/P42 (phospho-P44/P42, 9101, AB_331646) antibodies were from Cell Signaling Technology (Danvers, MA); β-actin (A5441, AB_476744) and β-tubulin (T4026, AB_477577) antibodies were from Sigma (St. Louis, MO); and anti-mouse (115-035-205, AB_2338513) and anti-rabbit (111-035-003, AB_2313567) HRP-conjugated IgG from Jackson (West Grove, PA). Protein band density was analyzed using UVP software (Version 6.7.4), using area density of equally sized rectangles encompassing the bands at the appropriate molecular weight, then normalized to the corresponding β-actin density and compared to control treatment by fold change.

2.3. Affymetrix Bovine Gene chip microarray

Each CL from the *in vivo* experiment described in Section 2.1 was homogenized and RNA was extracted using a Stratagene RNA Isolation Kit (Santa Clara, CA) following manufacturer's instructions. Quality of RNA was assessed by A260/280 ratio, only samples with ratios ≥ 2 were used for transcriptomics analyses. Samples were reverse transcribed to cDNA using iScript (Bio-Rad, Hercules, CA) and subjected to *in vitro* transcription per manufactures suggestion to generate biotinylated amplified RNA for hybridization using 3′ IVT Express (Affymetrix, Santa Clara, CA). Transcriptional changes were analyzed by hybridization of 500 ng biotinylated cDNA using Affymetrix (Santa Clara, CA) bovine whole-transcript microarray (Bovine Gene v1 Array [BovGene-1_0-v1]; GPL17645) at the University of Nebraska Medical Center Microarray Core Facility. Validation of target transcripts was performed after reverse transcription of 1 μg RNA using SuperScript II Reverse Transcriptase (Invitrogen, Grand Island, NY) followed by quantitative real-time PCR (qPCR) using gene-specific primers [Supplemental Table 1] on a CFX96 Touch™ Real-Time PCR Cycler (Bio-Rad, Hercules, CA) with SsoFast™ EvaGreen® Supermix (Bio-Rad, Hercules, CA). Comprehensive microarray methods and data are available in the Gene Expression Omnibus (GEO) database under accession GSE94069 and are described in the accompanying Data in Brief article (Talbott et al., 2017).

2.4. Microarray Statistics

The microarray data were preprocessed using the robust multi-array average (RMA) method from Affymetrix expression console software (Affymetrix Inc., Santa Clara, CA) to normalize data at the exon level. The mean intensities of multiple probe sets of the same gene were calculated under each array to obtain the corresponding gene expression intensities. The data was filtered to keep the genes with a raw expression value after preprocessing to be 10 or more for at least three of the 15 samples. Linear Models for Microarray Analysis (Smyth, 2004) in the Bioconductor suite (Gentleman et al., 2004) under the statistical program R (R Core Team, 2015) was applied to compare the log ratio between each of the PGF2α times and the saline control after adjusting for the box effect. Transcripts with a fold-change of at least 1.5 and a Benjamini-Hochberg adjusted *P*-value of less than 0.05 for each treatment condition versus control were identified as differentially expressed genes.

2.5. Self-organizing maps and statistics

Microarray data was filtered to keep genes with a raw expression value after preprocessing to be 30 or more for at least three of the 15 samples. The log ratio between each of the times and the

saline control were compared using Linear Models of Microarray Analysis in the Bioconductor suite in R. The self-organizing map (SOM) clustering algorithm GeneCluster 2.0 (Tamayo et al., 1999) was applied to differentially expressed genes that had a greater than 1.5-fold change in expression and *P*-value ≤ 0.05 between PGF2α-treated samples and the saline control. The mean normalized $\log_2$ intensity values from each of the five examined biological conditions were used as transcript expression profiles in the clustering analysis. The number of iterations in SOM clustering was set to 500,000 to generate SOMs and hierarchical clustering (correlation-based distance, average link).

2.6. Dataset comparisons

Two previously published microarray datasets, GSE23348 (Mondal et al., 2011) and GSE27961 (Shah et al., 2014) examined the effect of *in vivo* PGF2α (Lutalyse) or PGF2α analog (Juramate) treatment on the bovine luteal transcriptome using Affymetrix Bovine Whole Genome Gene Chips (GPL 2112). These datasets were chosen for comparison to the transcriptome dataset presented herein based on similarities in the experimental protocol comparing midcycle control CL expression profiles to CL profiles after treatment with PGF2α or analog for 4 h (GSE23348) or 6 h (GSE27961). Original. CEL and. CHP files were downloaded from the GEO database and processed as described in Section 2.4 *Microarray Statistics*. The differentially expressed mRNAs at 4 or 6 h were compared between the three microarray datasets to determine the similarities among the datasets.

2.7. Pathway analysis

Pathway analysis was evaluated using Ingenuity Pathway Analysis (IPA) [Application: Build: 430520M Copyright 2017 QIAGEN (Redwood City, CA)]. Transcripts found to be differentially

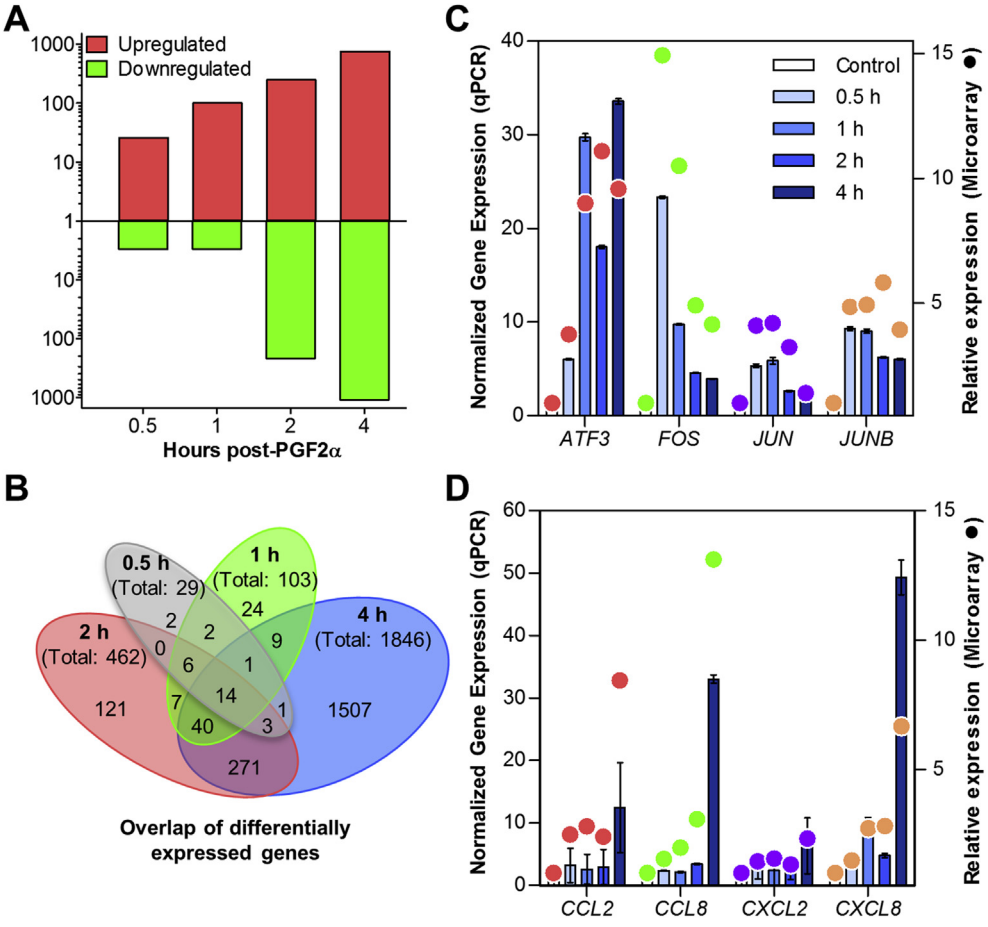

Fig. 1. Time-course of the transcriptomic response to PGF2α.
Midcycle cows (n = 3/time-point) were treated with 25 mg PGF2α for 0.5, 1, 2, and 4 h and control saline injections (n = 3). Samples were analyzed by Affymetrix bovine whole transcript microarray (Bovine Gene v1 Array [BovGene-1_0-v1]; GPL17645) and differentially expressed transcripts were identified based on fold change ≥ |1.5| and Benjamini-Hochberg adjusted *P*-value ≤ 0.05 compared to saline controls (n = 3). **(A)** Number of upregulated and downregulated differentially expressed transcripts at each time-point graphed on a log scale, upregulated transcripts appear in red above the central axis, and downregulated transcripts appear in green below the axis. **(B)** Venn diagram of the number of differentially expressed genes that overlapped between the four times examined. Each oval is labeled with the time-point and the total number of differentially expressed genes in the time-point. Overlapping parts of the ovals are labeled with the number of transcripts that were differentially expressed at the corresponding times. **(C & D)**. Quantitative PCR (qPCR) analysis of target genes normalized to *ACTB* and *GAPDH* expression and compared to saline controls using fold-change are displayed using bar graphs to represent mean ± SEM and plotted on the left Y-axis. Microarray determined fold-change of the target genes compared to control are overlayed using filled circles • to represent the mean (n = 3) and plotted on the right Y-axis. **(C)** Selected transcription factor genes (*ATF3*, *FOS*, *JUN*, and *JUNB*) were significantly different from control values ($P < 0.0001$) as determined by qPCR and determined as differentially expressed in the microarray (except *JUN* at 4 h). **(D).** Target chemokine transcripts (*CCL2*, *CCL8*, *CXCL2*, and *CXCL8*) were all upregulated at 4 h ($P < 0.01$). Additionally, *CXCL8* was significantly upregulated at 1 and 2 h ($P < 0.0001$, $P < 0.05$, respectively) as determined by qPCR. Determination of differentially expressed transcripts by microarray indicated significant upregulation of *CXCL2* and *CXCL8* at 4 h and *CCL8* at both 2 and 4 h. (For interpretation of the references to colour in this figure legend, the reader is referred to the web version of this article.)

expressed compared to saline-injected controls with ≥ 1.5-fold change and $P \leq 0.05$ were input into IPA for core analysis using Entrez gene IDs for evaluations of the time-course and comparison datasets. Unmapped genes ranged from 6.5 to 20.7% per individual times or datasets. Datasets were assessed for prediction of upstream regulators and signaling pathways. Additional pathway analysis was completed using DAVID (Version 6.8, released: Oct 2016) (Huang et al., 2009a, 2009b), Panther Database (Version 11.1, released: Oct 2016) (Mi et al., 2016, 2013; Thomas et al., 2006), and STRING Database (Version 10.0, released: Apr 16, 2016) (Szklarczyk et al., 2015) to validate IPA findings. Functional categorization of genes common to all three datasets examined was done by manual annotation of a single major functional category for each gene based on National Center for Biotechnology Information (NCBI), GeneCardsSuite descriptions and gene ontology (GO) annotations of genes.

3. Results

3.1. Bovine microarray

The analysis of the Affymetrix gene arrays revealed a total of 1654 differentially expressed gene transcripts. The number of differentially expressed genes increased during the time-course (Fig. 1A). Upregulated transcripts predominated at early times in response to PGF2α (89.6% and 97.1% upregulated, 0.5 and 1 h, respectively). Similar numbers of upregulated and downregulated transcripts were observed at 2 h after PGF2α (53.4% upregulated genes). Conversely, at 4 h after PGF2α, 58.2% of differentially regulated transcripts were downregulated. The overlap of altered transcripts among times is shown in a Venn diagram in Fig. 1B. Of note, 14 of the 29 differentially expressed mRNAs detected at 0.5 h after PGF2α were differentially expressed at all 4 times (Supplemental Table 2). Additionally, at 4 h after PGF2α, there were 1507 differentially expressed transcripts unique to that time-point. A full list of differentially expressed genes, fold changes and *P*-values is provided in Supplemental Table 2. Comprehensive microarray data can be found in the GEO database under accession GSE94069.

The top 10 upregulated and downregulated transcripts (by fold-change) at each time-point along with their fold change and *P*-values are listed in Tables 1 and 2, respectively. Transcription factors were particularly prominent early in the time-course response to PGF2α and although the number of transcription factors continued to increase, they made up a lower proportion of differentially expressed genes as the time-course proceeded [Fig. 1 in (Talbott et al., 2017)]. One-half hour after PGF2α treatment, 34.5% of the mapped differentially expressed genes had a transcription

Table 1
Top ten upregulated genes at each time-point[a].

	Gene Symbol	Entrez ID	Gene Name	Fold Change	*P*-value
0.5 h	*FOS*	280795	Fos proto-oncogene, AP-1 transcription factor subunit	14.94	8.22E-04
	NR4A1	528390	nuclear receptor subfamily 4 group A member 1	8.56	1.30E-05
	NR4A2	540245	nuclear receptor subfamily 4 group A member 2	7.34	4.94E-06
	NR4A3	528877	nuclear receptor subfamily 4 group A member 3	7.15	2.67E-04
	FOSB	540819	FosB proto-oncogene, AP-1 transcription factor subunit	6.74	2.40E-04
	APOLD1	538827	apolipoprotein L domain containing 1	6.57	8.33E-04
	IER2	525380	immediate early response 2	6.04	4.50E-05
	EGR1	407125	early growth response 1	5.57	2.40E-04
	JUNB	514246	JunB proto-oncogene, AP-1 transcription factor subunit	4.86	1.79E-06
	CYR61	508941	cysteine rich angiogenic inducer 61	4.61	3.03E-03
1 h	*NR4A3*	528877	nuclear receptor subfamily 4 group A member 3	27.85	7.81E-07
	FOSB	540819	FosB proto-oncogene, AP-1 transcription factor subunit	16.65	1.38E-06
	DUSP2	539140	dual specificity phosphatase 2	13.06	7.27E-05
	NR4A1	528390	nuclear receptor subfamily 4 group A member 1	11.36	1.38E-06
	EGR4	407155	early growth response 4	10.81	1.26E-04
	FOS	280795	Fos proto-oncogene, AP-1 transcription factor subunit	10.50	1.38E-03
	ATF3	515266	activating transcription factor 3	9.00	1.22E-05
	NR4A2	540245	nuclear receptor subfamily 4 group A member 2	8.84	9.30E-07
	ARC	519403	activity regulated cytoskeleton associated protein	7.06	4.02E-04
	DUSP5	507061	dual specificity phosphatase 5	6.55	9.51E-06
2 h	*EGR4*	407155	early growth response 4	20.38	1.44E-05
	FOSB	540819	FosB proto-oncogene, AP-1 transcription factor subunit	15.13	2.80E-06
	SERPINB2	505184	serpin peptidase inhibitor, clade B (ovalbumin), member 2	14.42	1.74E-04
	ARC	519403	activity regulated cytoskeleton associated protein	13.90	1.79E-05
	DUSP5	507061	dual specificity phosphatase 5	12.31	4.85E-07
	NR4A3	528877	nuclear receptor subfamily 4 group A member 3	11.77	1.49E-05
	F3	280686	coagulation factor III, tissue factor	11.10	1.89E-02
	ATF3	515266	activating transcription factor 3	11.09	4.85E-06
	INA	532236	internexin neuronal intermediate filament protein alpha	10.41	2.25E-03
	MMP12	526981	matrix metallopeptidase 12	10.26	2.11E-03
4 h	*MMP12*	526981	matrix metallopeptidase 12	41.71	1.06E-05
	SERPINB2	505184	serpin peptidase inhibitor, clade B (ovalbumin), member 2	25.49	1.31E-05
	SERPINE1	281375	serpin family E member 1	17.87	1.01E-06
	CSRP3	540407	cysteine and glycine rich protein 3	17.82	2.31E-04
	SERPINA14	286871	serpin peptidase inhibitor, clade A (alpha-1 antiproteinase, antitrypsin), member 14	17.57	2.58E-04
	IL33	507054	interleukin 33	17.46	1.76E-07
	IL1A	281250	interleukin 1 alpha	16.65	1.77E-05
	TNFSF18	768081	tumor necrosis factor superfamily member 18	15.38	1.60E-06
	DUSP5	507061	dual specificity phosphatase 5	14.52	1.23E-07
	INHBA	281867	inhibin beta A subunit	13.57	1.23E-07

[a] Top ten upregulated transcripts at each time examined, *P*-value ≤ 0.05, sorted from largest to smallest based on average fold change.

factor classification using DAVID molecular function analysis and at 4 h after PGF2α, only 1.9% of the differentially expressed genes were classified as transcription factors [Fig. 1 in (Talbott et al., 2017)]. Transcription factors that were upregulated at all times investigated included *ATF3, BTG2, FOS, FOSB, EGR3, JUNB, NR4A1, NR4A2, NR4A3,* and *ZFP36* (Supplemental Table 2). Verification of microarray results was completed using qPCR to verify the stimulation of several immediate-early response genes (*ATF3, FOS, JUN, JUNB*) which peaked between 1 and 2 h (Fig. 1C).

Several cytokine and chemokine-related transcripts were upregulated in response to PGF2α. At 2 h after PGF2α, upregulated cytokine and chemokine transcripts included *CCL8, IL1A, IL1B*, and *IL33* (Supplemental Table 2). Lastly, at 4 h, 25 cytokine and chemokine-related transcripts were upregulated including all of the upregulated cytokines and chemokines at 2 h and additionally including, *CCL2, CCL3, CCL4, CXCL2, CXCL5 CXCL8, CXCL13,* and *IL18* (Supplemental Table 2). Validation of selected cytokine and chemokines transcripts was performed by qPCR (Fig. 1D) and described by (Talbott et al., 2014). Suppressor of cytokine signaling 3 (*SOCS3*), which encodes a protein important in preventing over-activation of inflammatory conditions, was the first inflammatory/cytokine related transcript significantly upregulated at 1 h. At the 2 and 4 h times, both *SOCS3* and *SOCS1* were upregulated (Supplemental Table 2).

Downregulated genes included *NR5A2* (also known as *LRH1*) (Supplemental Table 2); however, many of the downregulated genes have no known role in luteal function or luteolysis. Analysis by IPA of downregulated genes indicated activation of 'decreased size of body' (z-scores; −4.029 and −8.795 at 2 and 4 h, respectively). Upstream regulators included activation of NUPR1 (z-scores; 2.53, 4.01 at 2 and 4 h, respectively) and inhibition of vascular endothelial growth factor (VEGF), upstream transcription factor 1 (USF1), and endothelin 1 (EDN1) (z-scores at 4 h; −4.55, −2.58, −2.43, respectively). Functional analysis by DAVID of downregulated genes at 4 h indicated an enrichment in insulin signaling and cyclic adenosine monophosphate signaling and metabolic processes.

3.2. Functional luteolysis

Serum progesterone was significantly decreased by PGF2α treatment at 2 and 4 h (51% and 54%, respectively) compared to saline-treated midcycle cows (Fig. 2A). Cows from different treatment groups were not different in age, weight or number of calves produced. There were no significant differences among groups in CL weight, ovary dimensions, and antral follicle counts [Fig. 2 in (Talbott et al., 2017)]. Despite the decrease in progesterone secretion by 2 h after PGF2α, there were no changes within our study in transcripts of proteins that directly control progesterone synthesis (Fig. 2B). The proteins encoded by *StAR, CYP11A1,* and *HSD3B1* (steroidogenic acute regulatory protein, cytochrome P450 family 11 subfamily A member 1, and hydroxyl-δ-5-steroid dehydrogenase, 3 β and steroid δ-isomerase 1, respectively) are directly responsible for the modification of cholesterol to progesterone, but the abundance of the transcripts were not changed following PGF2α treatment. Additionally, no changes were observed in the luteinizing hormone/chorionic gonadotropin receptor (*LHCGR*) or lipoprotein receptors: *SCARB1,* and *LDLR* (scavenger receptor class B member 1, and low density lipoprotein receptor) (Fig. 2B).

Conversely, several transcripts associated with cholesterol availability were differentially regulated (Fig. 2B). Transcript abundance of lipase E, hormone sensitive type (*LIPE*), which encodes the cholesteryl esterase hormone sensitive lipase (HSL) was decreased at 2 and 4 h. As well, the LDLR adaptor protein (*LDLRAP1*) transcript abundance decreased beginning at 2 h. Other genes with products influencing cholesterol availability that increased during the time-course included insulin induced gene 1 (*INSIG1*) and cholesterol 25-hydroxylase (*CH25H*) transcripts. Finally, there were no changes observed in transcript abundance of genes for reverse cholesterol transport proteins (*ABCA1, ABCG1, NR1H2, NF1H3,*

Table 2
Top ten downregulated genes at each time-point.

	Gene Symbol	Entrez ID	Gene Name	Fold Change	P-value
0.5 h	*LOC100337120*	100337120	T-cell activation Rho GTPase-activating protein-like	−3.81	4.47E-03
	LOC783362	783362	uncharacterized LOC783362	−3.81	3.25E-03
	MIR2450B	100313224	microRNA 2450b	−3.46	8.13E-03
1 h	*GBP4*	100298387	guanylate binding protein 4	−2.56	3.74E-02
	ARHGAP25	534994	Rho GTPase activating protein 25	−2.06	8.59E-03
	CARD6	520291	caspase recruitment domain family member 6	−1.75	3.74E-02
2 h	*GRIA1*	529618	glutamate ionotropic receptor AMPA type subunit 1	−4.57	3.26E-02
	LOC783362	783362	uncharacterized LOC783362	−4.24	7.48E-04
	CEP295NL	100125412	CEP295 N-terminal like	−3.95	3.30E-02
	CALB2	513947	calbindin 2	−3.57	1.63E-02
	LOC510193	527460	apolipoprotein L3	−3.41	4.43E-02
	LOC100337457	100337457	solute carrier family 23 member 2	−3.23	3.33E-02
	FAM13C	540918	family with sequence similarity 13 member C	−3.20	2.88E-03
	LOC100337120	100337120	T-cell activation Rho GTPase-activating protein-like	−3.04	6.89E-03
	RUNDC3B	525116	RUN domain containing 3B	−2.82	7.69E-03
	SDPR	532333	serum deprivation response	−2.78	7.24E-03
4 h	*LOC783362*	783362	uncharacterized LOC783362	−4.77	1.44E-04
	APLNR	615435	apelin receptor	−4.20	5.10E-04
	FOXL2	281770	forkhead box L2	−4.16	3.35E-06
	ARHGAP20	515501	Rho GTPase activating protein 20	−4.05	3.06E-04
	PIEZO2	522631	piezo type mechanosensitive ion channel component 2	−3.80	2.39E-04
	NPNT	513362	nephronectin	−3.69	8.59E-04
	GPAM	497202	glycerol-3-phosphate acyltransferase, mitochondrial	−3.55	7.42E-03
	LRIG3	506574	leucine rich repeats and immunoglobulin like domains 3	−3.50	5.31E-04
	MAMSTR	505540	MEF2 activating motif and SAP domain containing transcriptional regulator	−3.38	9.54E-04
	TNS3	516555	tensin 3	−3.31	8.60E-05

*Top ten downregulated transcripts at each time examined, *P*-value ≤ 0.05, sorted from largest to smallest decrease compared to control based on average fold change.

APOA1, and *APOE*) except *ABCA1*, which was reduced at 4 h (Fig. 2B).

3.3. Pathway analysis of the response to PGF2α

Ingenuity Pathway Analysis identified known PGF2α mediators including PGF2α itself (identified in IPA as the synthetic PGF2α, dinoprost), PKC group (Chen et al., 2001), ERK/MAPK (Arvisais et al., 2010; Chen et al., 2001, 1998; Yadav et al., 2002), and Ca^{2+} (Davis et al., 1987). All of these known PGF2α signaling intermediates were predicted as activated by IPA and the activation z-scores for each of these mediators are graphically represented in Fig. 3A. Most of these upstream regulators were predicted to have the greatest effect at 2 h. A curated list of upstream regulators predicted by IPA to be involved during the PGF2α time-course is available in Supplemental Table 1 in (Talbott et al., 2017).

Upstream regulator analysis predicted TNFα, IL-1β, IL-6 and IL-17A as active upstream regulators during the short time-course. Fig. 3B displays the activation z-scores of several inflammatory cytokines during the 4-h time-course demonstrating that activation scores for these inflammatory cytokines increased throughout the study. Both NF-κB and signal transducer and activator of transcription 3 (STAT3) were predicted to be activated during PGF2α –induced luteal regression (Fig. 3C). Additionally, inhibitors of cytokine signaling, SOCS1 and SOCS3 were predicted to be inhibited (Fig. 3C).

To test whether PGF2α or the predicted cytokines were capable of activating NF-κB, dispersed luteal cells from midcycle CL or enriched preparations of SLCs and LLCs were treated with PGF2α or select cytokines and acute activation of NF-κB and ERK pathways were examined. Treatment with PGF2α did not alter phosphorylation of the NF-κB subunit P65 but rapidly stimulated ERK phosphorylation in midcycle luteal cells (Fig. 3D). Fig. 3E illustrates that TNFα, IL-1β, and IL-17A consistently stimulated the phosphorylation of NF-κB P65 in dispersed mid-cycle luteal cells. The cytokines, TNFα, IL-1β, and IL-17A stimulated phosphorylation of P65 in both SLC and LLC, and PGF2α selectively stimulated ERK phosphorylation in LLC but had no effect on P65 (Fig. 3F). Interleukin-6 did not stimulate phosphorylation of ERK or P65 NF-κB as it is known to activate the JAK/STAT signaling pathway (Schaper and Rose-John, 2015).

Ingenuity Pathway Analysis highlighted canonical pathways predicted to be activated or inhibited within this dataset based on the downstream targets' differential expression (*P*-value) and direction of change (z-score). The top five canonical pathways (by z-score then *P*-value) identified from each time-point are listed in Table 3 and a more extensive list can be seen in Table 1 in (Talbott et al., 2017). At 0.5 h after PGF2α, no pathways had a z-score $\geq |2|$, likely due to the small number of differentially expressed genes. However, several pathways had *P*-values ≤ 0.05, including 'NRF2-mediated Oxidative Stress Response'. Seven pathways were predicted as activated at the 1 h time-point. At 2 h after PGF2α, five pathways were predicted as activated and at 4 h after PGF2α, 20 pathways were identified (5 activated and 15 inhibited). Two canonical pathways were predicted to be activated in 2 of the 4 times examined, 'cholecystokinin/gastrin-mediated signaling', and 'Toll-like receptor signaling'. Several additional canonical pathways including, 'Acute Phase Response Signaling', 'ILK Signaling', and 'TGF-β Signaling' were identified that had z-scores $\geq |1|$ in at least two times [Table 1 in (Talbott et al., 2017)].

3.4. PGF2α activates well-organized transcriptional cascades

Ten self-organizing maps (SOMs) were generated based on transcripts that had similar changes in their expression profiles relative to control throughout all four times. The differentially expressed transcripts included in each SOM are found in Supplemental Table 3. Of these, two SOMs reflected the expression patterns of immediate-early response genes (Fig. 4A & F) and reached peak levels in 1–2 h and then returned toward baseline. Four SOMS corresponded to early and delayed-early responsive transcripts with changes in mRNA abundance early in the time-

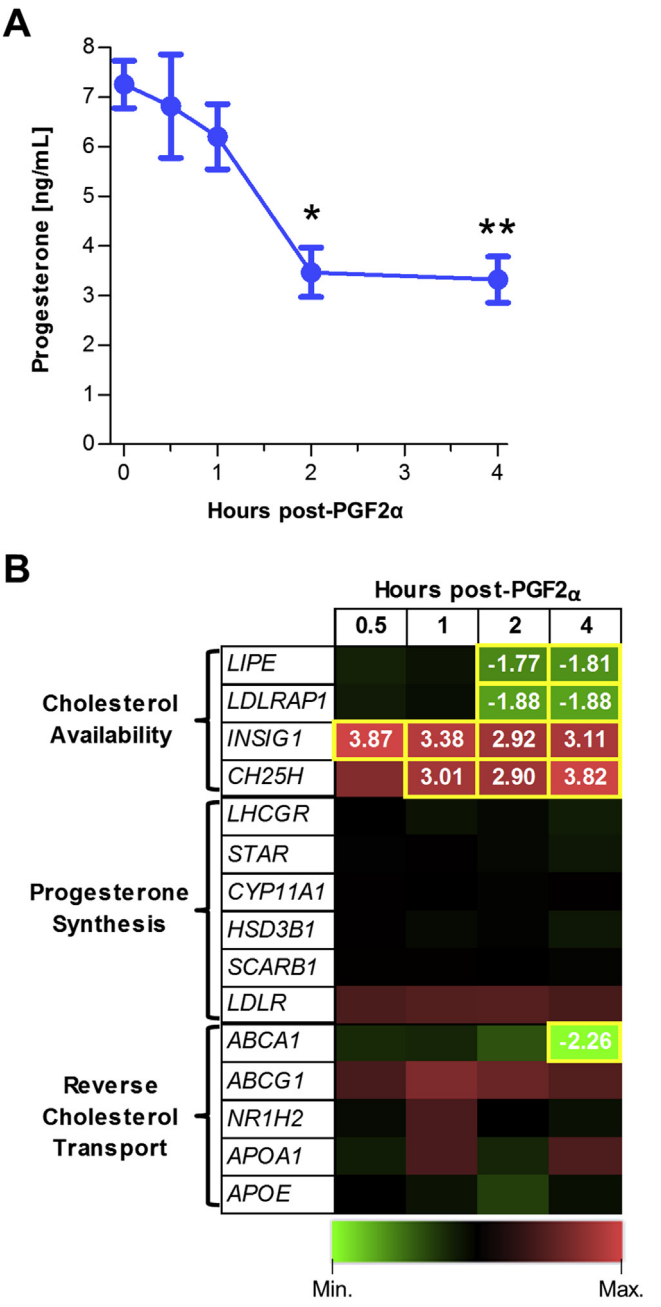

Fig. 2. PGF2α induced reductions in serum progesterone are correlated with reductions in the expression of genes that control intracellular cholesterol availability.

(A) Serum progesterone concentrations of cows 0.5–4 h after PGF2α treatment (n = 3/time-point). *P ≤ 0.05, **P ≤ 0.01 compared to saline-treated animals. **(B)** Heat map of genes that regulate cholesterol availability, progesterone synthesis, and reverse cholesterol transport. Green indicates decreased and red indicates increased transcripts over control. Yellow boxes indicate times that were significantly altered from saline controls and fold changes from saline controls are indicated in the respective boxes. (For interpretation of the references to colour in this figure legend, the reader is referred to the web version of this article.)

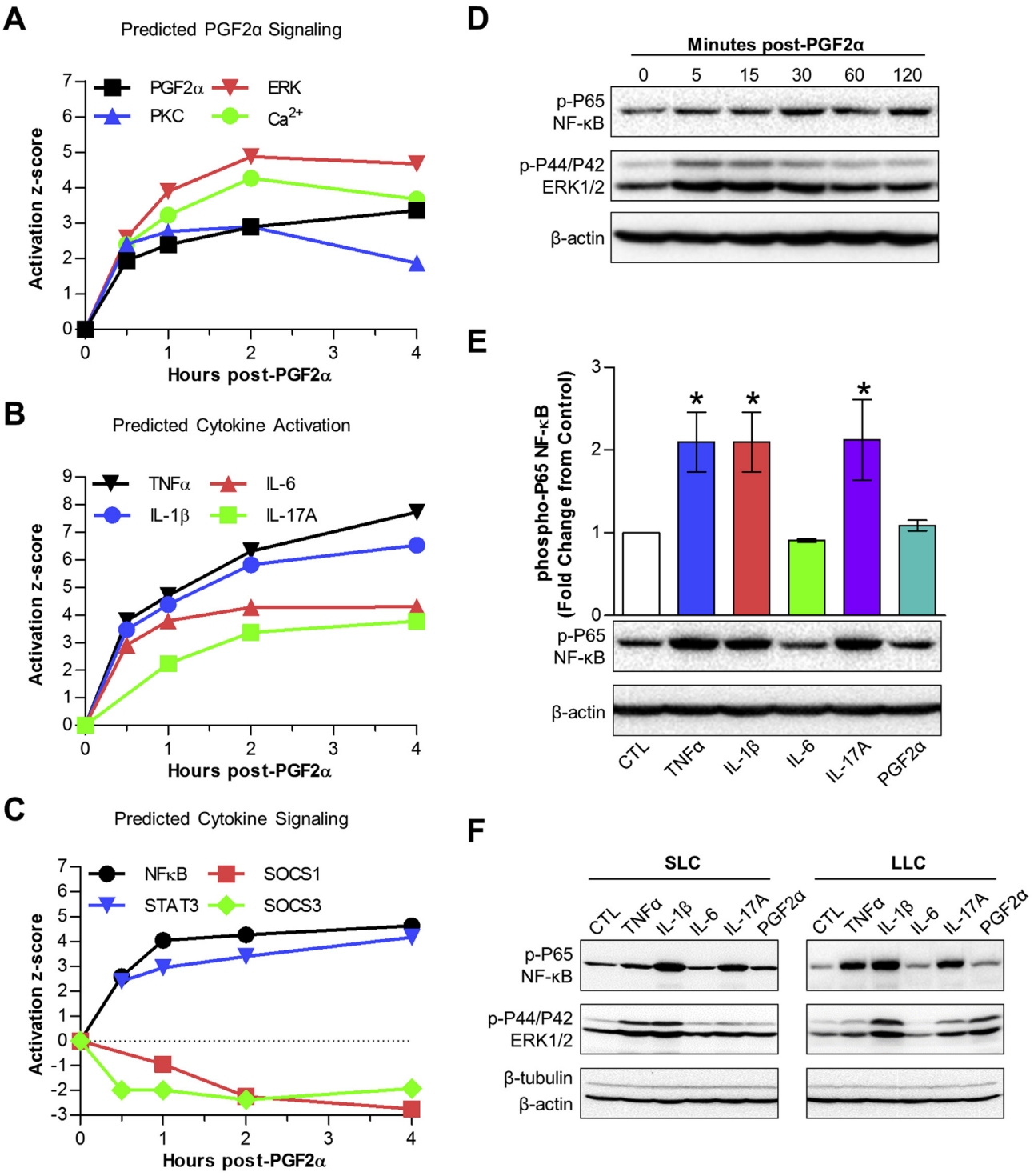

Fig. 3. ***In vivo*** **treatment with PGF2α predicts classical PGF2α and cytokine signaling.**
(A, B & C) The activation z-score of specific upstream regulators, determined by IPA, graphed against time. **(A)** Classic mediators of PGF2α signaling including, PGF2α itself (dinoprost, black), protein kinase C (PKC group, blue), ERK (red), and Ca^{2+} (green). **(B)** Cytokine activation scores including, TNFα (black), IL-1β (blue), IL-6 (red), and IL-17 (green). **(C)** Cytokine signaling molecules: NF-κB (black), STAT3 (blue), and suppressors of cytokine signaling, SOCS1 (red) and SOCS3 (green). **(D)** Phospho-P65 quantification (mean ± SEM) of non-pregnant midcycle luteal cells (n = 3) treated with TNFα, IL-1β, IL-17A and PGF2α for 30 min followed by Western blot analysis, normalized to β-actin and compared to untreated controls, representative immunoblots are shown below the bar graph. *$P \leq 0.05$ compared to control. **(E)** Western blot of non-pregnant midcycle luteal cells treated with PGF2α for the indicated times immunoblotted for phospho-P65, phospho-ERK1/2, β-tubulin, and β-actin. **(F)** Western blot of small luteal cells (SLC) and large luteal cells (LLC) treated with TNFα, IL-1β, IL-6, IL-17A (10 ng/mL each) and PGF2α (100 nM) for 30 min and immunoblotted for phospho-P65, phospho-ERK1/2, β-tubulin, and β-actin. (For interpretation of the references to colour in this figure legend, the reader is referred to the web version of this article.)

course (but less rapid than the immediate early-response genes) which either plateaued (Fig. 4B and G) or continued to change throughout the examined time frame (Fig. 4C and H). Finally, there were two SOMs where changes in transcript abundance did not

begin until the 2-h time-point indicative of late-response genes (Fig. 4D and I). Two additional SOMs had biphasic transcript profiles, which changed early (either up- or downregulated), returned to baseline and then rebounded at later times (Fig. 4E and J).

Upregulated SOMs had several common IPA-predicted upstream regulators such as TNFα, TGFβ, IL-1β, and NF-κB (Fig. 4 and Supplemental Table 2 in (Talbott et al., 2017)). Downregulated SOMs had common inhibition predictions of VEGF, PPAR ligands, and T3 (the thyroid hormone, triiodothyronine) (Fig. 4 and Supplemental Table 2 in (Talbott et al., 2017)). Functional analysis by IPA of the genes in each SOM predicted activation of 'migration of cells' and inhibition of organismal death in immediately-early upregulated genes (Supplemental Table 3 in (Talbott et al., 2017)). Early and delayed-early upregulated gene patterns had functional predictions of 'cell survival' (Supplemental Table 3 in (Talbott et al., 2017)). Late upregulated gene patterns were consistent with increases in 'migration of cells' and biphasic upregulated genes had functional predictions of inhibited 'organismal death' (Supplemental Table 3 in (Talbott et al., 2017)). Downregulated SOMs had functional predictions of 'organismal death' for immediate-early and downregulated gene patterns (Supplemental Table 3 in (Talbott et al., 2017)). Functional annotations predicted activation of 'organismal death' in delayed-early downregulated SOM, increased 'morbidity or mortality' in late downregulated genes, and death and increased 'organismal death' in biphasic downregulated genes (Supplemental Table 3 in (Talbott et al., 2017)). Upstream regulators and functions of individual SOMs derived from IPA are available in Supplemental Table 2 and 3 in (Talbott et al., 2017).

Functional annotations of each SOM revealed that SOMs, which peaked early, had a greater proportion of genes with a 'regulation of gene expression' biological process annotation by DAVID; including, within the immediate early categories 47.2% of up- and 18.2% of downregulated genes. In the early responses, 'regulation of gene expression' composed of 31.4% of upregulated and 22.9% of downregulated genes. Within the delayed-early SOMs, 19.2% of up- and 22.3% of downregulated genes were also annotated with 'regulation of gene expression'. Whereas, late response gene patterns had fewer genes classified as 'regulation of gene expression' compared to earlier gene profiles (18.2% up- and 19.6% downregulated). Instead, delayed-early and late upregulated SOMs had 7.1% of genes associated with "inflammatory reactions" (*P*-values: 1.50E-05, 9.50E-08, DAVID). Biphasic upregulated genes had biological process annotations including immune response-activating signal transduction. Finally, biphasic downregulated genes had annotations related to fibrosis. Of the downregulated SOMs, several contained components of PPAR signaling and VEGF signaling.

3.5. Dataset comparisons

Two previously published microarray datasets GSE23348 (Mondal et al., 2011) and GSE27961 (Shah et al., 2014) examined the effect of *in vivo* PGF2α treatment on midcycle bovine CL and similarities in the experimental design allowed direct comparison of the present study with the previous two microarray datasets. Mondal et al. collected luteal tissue from Angus crossbred heifers 4 h after giving an intramuscular injection of 25 mg Lutalyse at day 11 of the estrous cycle. Shah et al. treated non-lactating *Bubalus bubalis* (water buffalo) cows with a 500 μg dose of Juramate (equivalent to 25 mg of Lutalyse (Salverson et al., 2002)) and collected luteal tissue at 6 h after PGF2α. The overlap of differentially expressed transcripts between the three datasets is visually represented in a Venn diagram in Fig. 5A. Comparison of the three datasets revealed 515 genes found by at least 2 of the 3 studies (Supplemental Table 4), and 124 genes that were similarly altered in all the datasets including 43 upregulated genes and 81 downregulated genes (Table 4).

Independent bioinformatics analysis of each dataset revealed common regulatory elements. First, IPA predicted similar upstream regulators in each dataset such as PKC, MAPK/ERK, TNFα, IL-1α/β, and IL-17 [Table 3 in (Talbott et al., 2017)]. Canonical pathway analysis of each of the three datasets commonly predicted activation of triggering receptor expressed on myeloid cells 1 (TREM1) signaling, an important pathway for activation of macrophages and neutrophils (Arts et al., 2013) [Supplemental Table 4 in (Talbott et al., 2017)]. Bioinformatic analysis of the 124 genes common to all 3 datasets indicated activation of FOS, JUNB, MAPK/ERK, IL-1β,

Table 3
Predicted canonical pathways activated during the early response to PGF2α treatment.

	Ingenuity Canonical Pathways	z-score	P-value	Molecules
0.5 h	NRF2-mediated Oxidative Stress Response		1.41E-02	*FOS, JUN, DNAJB1, JUNB*
	Corticotropin Releasing Hormone Signaling		1.41E-02	*FOS, JUN, NR4A1*
	IGF-1 Signaling		1.41E-02	*FOS, JUN, CYR61*
	IL-17A Signaling in Gastric Cells		1.41E-02	*FOS, JUN*
	PI3K Signaling in B Lymphocytes		1.41E-02	*FOS, JUN, ATF3*
1 h	ILK Signaling	2.449	2.34E-02	*FOS, JUN, SNAI1, MYC, SNAI2, RND3*
	Cholecystokinin/Gastrin-mediated Signaling	2	3.89E-02	*FOS, JUN, SRF, RND3*
	HMGB1 Signaling	2	2.45E-02	*FOS, JUN, SERPINE1, PLAT, RND3*
	Endothelin-1 Signaling	2	8.71E-02	*FOS, JUN, MYC, EDNRB*
	IL-8 Signaling	2	1.08E-01	*FOS, JUN, ANGPT2, RND3*
2 h	Cholecystokinin/Gastrin-mediated Signaling	2.646	2.99E-01	*FOS, JUN, SRF, IL1B, IL1A, RND3, IL33*
	Acute Phase Response Signaling	2.121	4.81E-01	*FOS, JUN, IL1B, JAK2, SOCS3, IL1A, SERPINE1, IL33*
	Toll-like Receptor Signaling	2	2.99E-01	*FOS, JUN, IL1B, IL1A, TRAF1, IL33*
	TGF-β Signaling	2	5.45E-01	*FOS, JUN, INHBA, SERPINE1*
	LPS/IL-1 Mediated Inhibition of RXR Function	2	7.43E-01	*JUN, IL1B, PPARGC1B, IL1A, NR5A2, IL33*
4 h	Death Receptor Signaling	−2.714	3.23E-01	*IKBKG, TANK, CFLAR, NFKB1, PARP1, PARP4, CASP9, NFKBIA, ACIN1, TNKS, BIRC3, SPTAN1*
	Integrin Signaling	−2.683	4.69E-01	*ASAP1, TLN1, RRAS2, ITGAV, ITGA2, CAPN1, TSPAN4, PXN, PIK3C2B, MYL9, PIK3R1, GAB1, ITGA9, SOS1, PIK3CG, RHOG, PIK3CA, ARHGEF7, MAP2K2, TSPAN5, PPP1CB, PLCG1, ACTN4*
	UVA-Induced MAPK Signaling	−2.496	1.64E-01	*SMPD2, MTOR, PARP4, RRAS2, CASP9, PIK3C2B, PIK3R1, GAB1, TP53, TNKS, PIK3CG, FOS, RPS6KA5, PARP1, PIK3CA, PLCG1*
	Retinoic acid Mediated Apoptosis Signaling	−2.449	1.78E-01	*CFLAR, PARP1, PARP4, CASP9, RXRB, CRABP2, RARG, TNKS*
	MIF Regulation of Innate Immunity	2.449	3.44E-01	*FOS, LY96, NFKB1, CD14, NFKBIA, TP53*

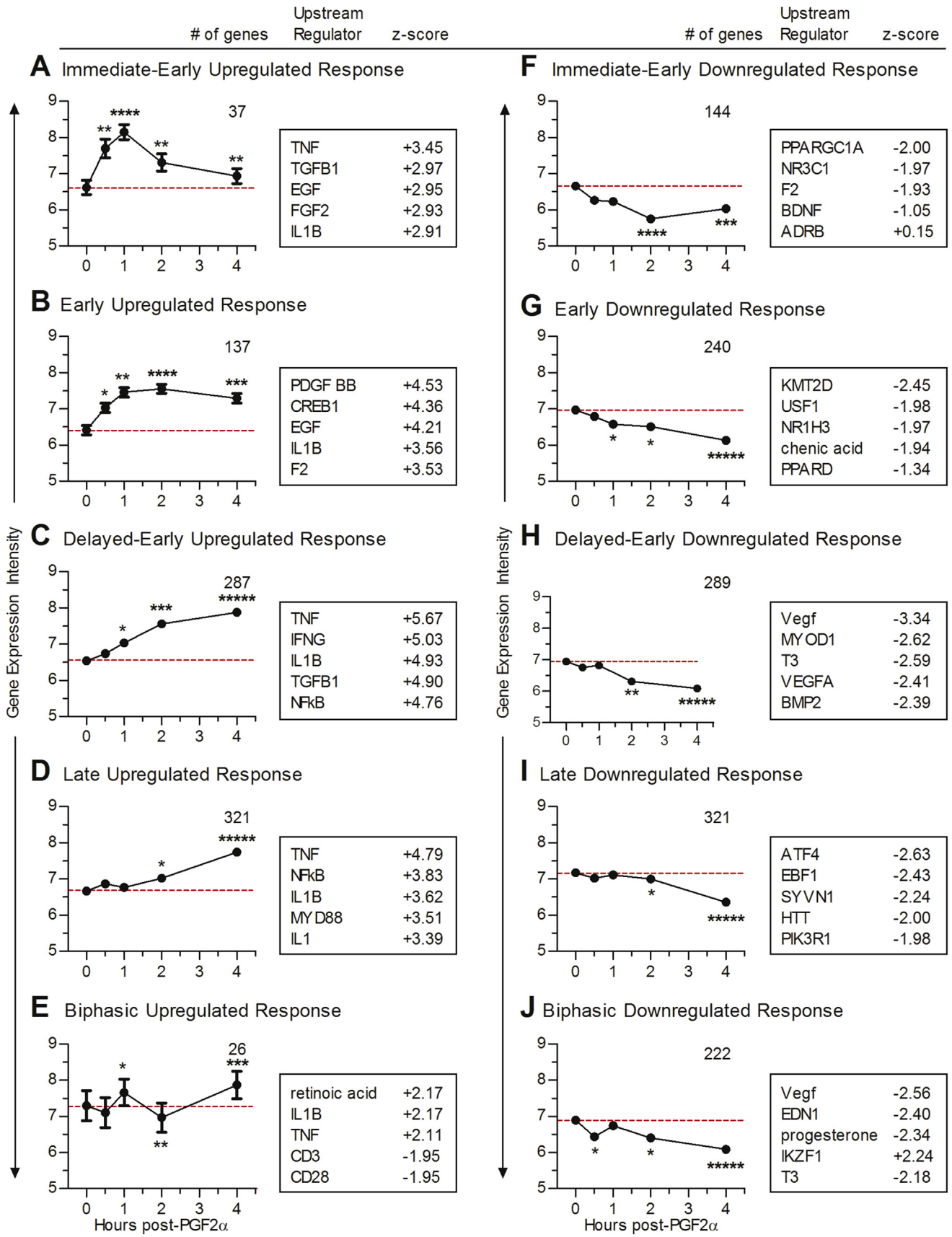
A Immediate-Early Upregulated Response
# of genes 37
Upstream Regulator z-score
TNF +3.45
TGFB1 +2.97
EGF +2.95
FGF2 +2.93
IL1B +2.91
B Early Upregulated Response
137
PDGF BB +4.53
CREB1 +4.36
EGF +4.21
IL1B +3.56
F2 +3.53
C Delayed-Early Upregulated Response
287
TNF +5.67
IFNG +5.03
IL1B +4.93
TGFB1 +4.90
NFkB +4.76
D Late Upregulated Response
321
TNF +4.79
NFkB +3.83
IL1B +3.62
MYD88 +3.51
IL1 +3.39
E Biphasic Upregulated Response
26
retinoic acid +2.17
IL1B +2.17
TNF +2.11
CD3 -1.95
CD28 -1.95
F Immediate-Early Downregulated Response
144
PPARGC1A -2.00
NR3C1 -1.97
F2 -1.93
BDNF -1.05
ADRB +0.15
G Early Downregulated Response
240
KMT2D -2.45
USF1 -1.98
NR1H3 -1.97
chenic acid -1.94
PPARD -1.34
H Delayed-Early Downregulated Response
289
Vegf -3.34
MYOD1 -2.62
T3 -2.59
VEGFA -2.41
BMP2 -2.39
I Late Downregulated Response
321
ATF4 -2.63
EBF1 -2.43
SYVN1 -2.24
HTT -2.00
PIK3R1 -1.98
J Biphasic Downregulated Response
222
Vegf -2.56
EDN1 -2.40
progesterone -2.34
IKZF1 +2.24
T3 -2.18
Gene Expression Intensity
Hours post-PGF2α

TNFα, TGFβ, IL-6 (Fig. 5B) as well as canonical pathways like IL-6 Signaling, Acute Phase Response Signaling, and NF-κB Signaling Table 3 in (Talbott et al., 2017). Curated lists of canonical pathway and upstream regulator predictions by IPA from the 124 genes common to all 3 datasets are available in Table 3 and Supplemental Table 5 in (Talbott et al., 2017). Pathway analysis of the 124 common genes by IPA, DAVID, Panther, and String consistently reported enrichment of TGFβ signaling (4 of 4) and p53 signaling (3 of 4) [Table 4 in (Talbott et al., 2017)]. Finally, functional analysis indicated groups of genes involved in cell-cell interaction (12.9%), cytokine signaling (8.9%), and transcriptional regulation (8.1%) in Fig. 5C. The genes in each functional category are listed in Table 4.

4. Discussion

4.1. Overview of study

This study uses a systems biology approach to provide a detailed understanding of the early (0.5–4 h) transcriptional effects that occur during PGF2α-induced luteolysis *in vivo*. Our analysis predicts activation of cytokines (TNFα, IL-1β, IL-6, IL-17A, & IL-33) and cytokine signaling intermediates (NF-κB, STAT) early in the time-course. However, changes in cytokine transcripts are not apparent until 2–4 h after PGF2α. The effects of PGF2α *in vivo* may require the activation of secondary mediators, such as cytokines, which activate NF-κB and STAT signaling because PGF2α is unable stimulate of NF-κB P65 phosphorylation in isolated luteal cells. The rapid influx of various immune cells in response to the initiation of luteolysis (Penny et al., 1999; Shirasuna et al., 2012b) and the release of preformed cytokines could explain the prediction of cytokine signaling effects very early in the PGF2α response. As well, the activation of NF-κB signaling could contribute to later responses seen after PGF2α administration.

Analysis of gene expression changes confirms changes in the transcriptome that are consistent with PGF2α signaling, including the rapid induction of immediate-early response genes (*ATF3*, *EGR1*, *FOS*, *JUN*, and *NR4A2*) (Atli et al., 2012; Chen et al., 2001; Mao et al., 2013). Bioinformatics analysis also identifies upstream regulators consistent with known PGF2α signaling mediators such as dinoprost (PGF2α), PKC, Ca^{2+}, and ERK. The bioinformatics findings indicating activation of classical PGF2α signaling pathways after *in vivo* treatment are an important validation of the predictive power of the bioinformatics tools used in this study. Comparison with similar datasets (Mondal et al., 2011; Shah et al., 2014) yields comparable results, predicting both PGF2α signaling and cytokine signaling in the CL after PGF2α treatment.

4.2. Induction of functional luteolysis

In this study, *in vivo* administration of PGF2α decreases serum progesterone within 2 h of treatment. Though, serum progesterone concentrations did not fall below 1 ng/mL, a cutoff that indicates irreversible functional regression, which typically occurs 18–24 h after the onset of luteolysis (Acosta et al., 2002; Levy et al., 2000). Additionally, there are no changes in CL weight, indicating that structural regression of the CL has not yet begun. The reduction in serum progesterone concentrations is not accompanied by reductions in the expression of the steroidogenic enzymes: *StAR, CYP11A1,* and *HSD3B1*. Furthermore, transcripts for key receptors (*LHCGR*, *SCARB1*, or *LDLR)* intimately involved in progesterone synthesis are also unchanged. These findings showing a marked reduction in serum progesterone prior to changes in steroidogenic gene transcript abundance are similar to other studies (Atli et al., 2012; Mondal et al., 2011; Shah et al., 2014). However, it is possible that changes in abundance or function of specific proteins may occur prior to down-regulation of the corresponding mRNA (Shah et al., 2014).

These observations suggest that alternate pathways could contribute to the early reduction in luteal progesterone synthesis. Based on our findings, it seems possible that the decrease in *LIPE* could contribute to the decrease in progesterone production because its protein product, HSL, interacts directly with lipid droplets to hydrolyze cholesteryl esters to liberate cholesterol for steroidogenesis (Manna et al., 2013). Decreases in *LDLRAP1* could inhibit progesterone production by reducing the cholesterol available for use in the cell since endocytosis of LDL particles requires the LDLRAP1 cofactor (Sirinian et al., 2005). An increase in INSIG1 concentrations could affect steroidogenesis through suppressing transcription of *de novo* cholesterol synthesis and uptake proteins, (Sun et al., 2005); however, *de novo* synthesis is not a primary source of cholesterol for steroidogenesis in the CL (O'Shaughnessy and Wathes, 1985). Finally, increases in CH25H could catalyze the hydroxylation of cholesterol to 25-hydroxycholesterol which is a potent inhibitor of *de novo* cholesterol synthesis (Lund et al., 1998). However, 25-hydroxycholesterol can also act as a substrate for steroidogenesis (Toaff et al., 1982) although it is unclear how physiological concentrations of this oxysterol would act on bovine luteal cells or neighboring cells. The reduction in *LIPE* expression together with alterations in *LDLRAP1*, *INSIG1*, and *CH25H* transcript abundance could have a combined negative effect on intracellular cholesterol availability.

Activation of reverse cholesterol transport could also effectively reduce intracellular cholesterol availability for progesterone synthesis. Other studies have reported an increase in reverse cholesterol transport transcripts such as *ABCA1, ABCG1, NR1H2, NF1H3, APOA1,* and *APOE* during luteolysis (Bogan and Hennebold, 2010; Seto and Bogan, 2015). However, in this dataset, only a single transcript of the reverse cholesterol transport process, *ABCA1,* changes compared to control, and it decreases. Thus, changes in transcript abundance that contribute to increases in reverse cholesterol transport do not appear to contribute to the early reductions in circulating progesterone, but may play important roles later in luteal regression.

4.3. Cytokine signaling

The present study implicates IL-33 and IL-17 cytokines as potential regulators of luteal regression, although neither have

Fig. 4. Temporal response waves to PGF2α.
Self-organizing maps (SOMs) graphs were generated as detailed in Methods. Each graph shows the average log2 transcript expression intensity ± SEM of the transcripts grouped into each SOM. Red dashed lines demonstrate the average transcript expression intensity at baseline. Numbers in the upper right of the individual graphs represent the number of transcripts within each SOM. Groups of transcripts that were upregulated during the PGF2α time-course are shown on the left **(A, B, C, D, & E)** and downregulated transcripts on the right **(F, G, H, I, & J)**. **(A & F)** SOMs showed responses typical of immediate-early response genes, peaked between 1 and 2 h and returned to baseline. **(B & G)** SOMs demonstrated early response genes, peaked at 2 h and maintained through the 4-h time-point. **(C & H)** SOMs demonstrated delayed-early response genes, which gradually moved away from baseline throughout the time-course. **(D & I)** SOMs showed late-response genes, which stayed near the baseline and then began changing at 2–4 h **(E & J)** Biphasic SOMs, which had an early change in transcript expression, returned to baseline and then had a second change in transcription levels. Boxes to the right of the graphs include the top upstream regulators predicted to be involved using IPA at the peak of change from controls, along with their corresponding IPA determined activation z-score. Data points in each SOM are labeled to indicate the percentage of transcripts that are differentially expressed at each time-point: ***** 99–100%; **** 76–98%; *** 51–75%, ** 26–50%, * 1–25%. (For interpretation of the references to colour in this figure legend, the reader is referred to the web version of this article.)

A Overlap of differentially expressed genes

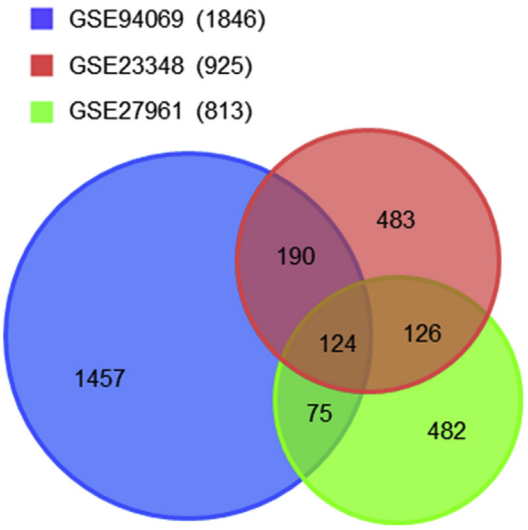

B Top Upstream Regulators for Common Genes

Molecule	Molecule Type	Z-score
IL1B	Cytokine	4.050
TNF	Cytokine	3.846
TGFB1	Growth factor	3.571
EDN1	Cytokine	3.551
F2	Peptidase	3.390
FGF2	Growth factor	3.000
EGF	Growth factor	2.997
HIF1A	Transcription regulator	2.976
IL6	Cytokine	2.969
MYD88	Other (NF-κB regulator)	2.961
CTNNB1	Transcription regulator	2.939
IL1	Group	2.935
NUPR1	Transcription regulator	2.887
PDGF BB	Complex	2.851
ERK	Group	2.771

C Functions of Common Genes

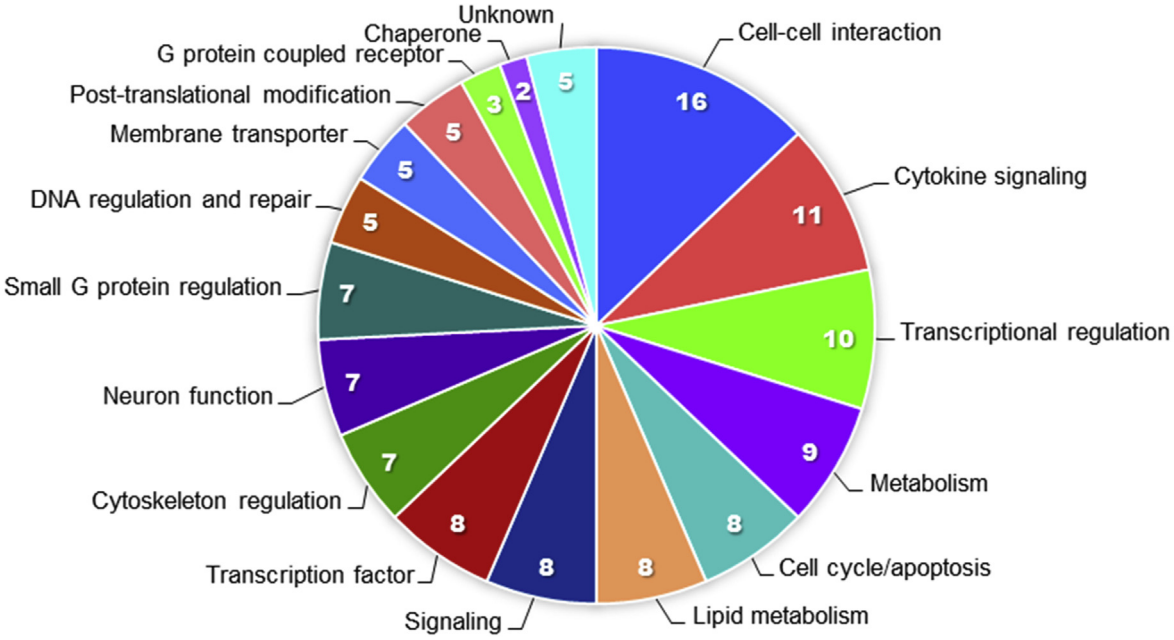

Fig. 5. Common gene alterations in response to PGF2α.
(A) Venn diagrams demonstrate the number of differentially expressed genes that overlapped between the three examined datasets GSE94069 (blue, Talbott et al., 2017), GSE23348 (red, Mondal et al., 2011), and GSE27961 (green, Shah et al., 2014). The legend indicates the numbers of total differentially expressed genes in parentheses for each dataset. Overlapping parts of the circles are labeled with the corresponding number of transcripts that are differentially expressed in that situation. **(B)** The top 15 IPA-predicted upstream regulators based on the 124 common genes with corresponding IPA molecule type designations and z-scores. **(C)** Functional categorization of the 124 common genes common to all three datasets, sections are labeled with both the category and the number of genes in each category. (For interpretation of the references to colour in this figure legend, the reader is referred to the web version of this article.)

previously been proposed to have a role in luteolysis. Nevertheless, *IL33* transcripts increase 17-fold over controls and is upregulated in all three datasets. Two recent reports indicate that IL-33 may play a role in follicular atresia (Carlock et al., 2014; Wu et al., 2015) and we propose that IL-33 could play a similar role in luteal regression. Preliminary data in our laboratory indicates that IL-33 does not have a direct effect on *in vitro* primary luteal cell cultures (not shown), presumably because luteal cells lack or have a low

Table 4
Common transcripts differentially expressed in response to PGF2α treatment.

Gene	Entrez Gene ID	Fold Change		
		GSE94069	GSE23348	GSE27961
Cell-cell interaction				
SERPINB2	505184	25.49	5.27	5.10
SERPINE1	281375	17.87	28.96	31.00
AMIGO2	514273	8.27	8.65	8.09
PLAUR	281983	6.83	5.92	7.39
SDC4	508133	6.59	8.44	19.13
HS3ST5	540355	4.77	7.73	9.33
MMP1	281308	4.11	12.26	6.44
THBS1	281530	2.89	2.02	3.90
CLDN1	414922	2.65	3.52	3.23
CD44	281057	2.49	3.44	8.22
CLDND1	515537	2.45	1.55	1.79
ITGAV	281875	1.75	1.93	2.79
EMCN	616367	−2.05	−1.55	−2.74
CLIC5	281696	−2.41	−1.69	−2.19
TMEM204	615464	−2.83	−1.72	−1.89
NPNT	513362	−3.69	−2.33	−2.51
Cytokine signaling				
IL33	507054	17.46	6.92	2.96
INHBA	281867	13.57	19.69	27.25
SPP1	281499	5.73	7.55	4.65
MT2A	404070	3.56	4.65	3.99
BAMBI	530147	3.41	1.57	2.99
NRG1	281361	3.14	2.15	8.78
IL18	281249	3.08	2.53	2.50
BMP2	615037	3.02	5.47	3.92
STAMBP	532672	1.82	1.98	3.19
CD14	281048	1.81	2.48	3.68
PDGFC	613787	1.70	1.77	1.78
Transcriptional Regulation				
ELL2	782605	2.30	2.15	4.06
HMGA1	618849	1.86	4.11	3.71
AGO2	404130	1.75	2.03	2.41
RPF2	511294	1.59	1.62	1.50
EIF4A1	504958	1.56	1.53	1.71
CPEB2	538880	−1.63	−1.95	−1.67
POLR1E	511587	−1.65	−1.90	−2.53
DCP1B	514548	−1.71	−1.54	−1.95
HEXIM1	539696	−2.88	−2.24	−2.37
ZMYM3	522721	−3.11	−2.18	−2.62
Metabolism				
ARG2	518752	5.95	2.56	3.95
GCNT4	782825	4.47	2.84	3.18
HK2	788926	3.50	3.61	4.24
LDHA	281274	1.77	1.54	2.32
PDP1	280891	1.64	1.50	2.02
RPIA	613376	1.52	1.68	2.04
METRNL	534297	1.52	1.89	2.11
PGM5	785045	−1.68	−1.73	−2.02
MPPED2	540914	−2.35	−1.60	−2.33
Transcription factor				
FOSL1	531389	2.85	2.80	3.19
BCL6	539020	2.69	3.49	2.23
SRF	533039	2.58	2.42	2.75
TGIF1	510050	2.29	2.50	1.90
BZW2	326579	2.11	1.85	2.19
NR5A2	541305	−1.79	−2.27	−2.58
ZNF22	768051	−2.29	−1.68	−1.73
ZNF827	104974573	−2.30	−1.53	−1.67
Signaling				
PDE8A	506787	1.97	2.31	4.12
PDE4B	100124505	1.76	2.22	3.60
PPP4R4	537521	1.72	3.59	10.10
TMEM64	536822	1.62	1.70	1.69
PIK3CA	282306	1.54	1.57	1.80
EVC2	280834	−1.70	−1.52	−1.78
DACT1	538778	−2.18	−1.90	−1.75
TMEM88	507172	−2.76	−1.78	−2.75
Lipid metabolism				
OLR1	281368	9.18	14.54	15.84
SRD5A1	614612	2.43	2.31	4.57
SPHK1	618605	2.18	2.27	2.04
PITPNC1	782067	1.53	1.57	1.55
ABCD4	515848	−1.80	−1.80	−1.80
OXSM	513530	−1.86	−2.40	−2.14
MID1IP1	615572	−1.90	−1.89	−2.68
GPAM	497202	−3.55	−2.86	−2.34
Cell cycle/apoptosis				
CDKN1A	513497	4.16	3.67	2.55
TNFRSF12A	617439	2.63	2.45	4.22
BTG1	281032	2.58	1.80	2.29
CCNG2	512960	2.18	1.59	1.90
STK17A	513665	2.05	1.81	1.90
BTG3	541054	1.89	1.53	2.11
CCNYL1	538167	1.70	1.69	1.97
IFT122	536731	−1.53	−1.71	−1.64
Small G-protein regulation				
RASA2	533491	3.21	1.74	1.70
TIAM1	536517	2.28	3.43	2.38
RHOBTB1	540513	−1.85	−1.57	−2.49
WIPF3	786606	−1.90	−1.55	−2.13
AGFG2	510361	−2.08	−2.01	−1.93
RGL1	522344	−2.23	−1.58	−1.73
ARHGAP19	526945	−2.34	−2.02	−2.08
Neuron function				
GAL	280799	10.15	55.44	11.39
CA8	515918	2.97	3.60	6.36
STK38L	514787	2.05	1.54	1.85
SLITRK2	540117	2.01	4.08	6.64
PNMA1	538718	−1.98	−3.18	−1.83
SEMA6D	518458	−2.28	−2.05	−1.95
PTHLH	286767	−2.49	−3.91	−4.55
Cytoskeleton regulation				
Cnn1	534583	5.19	6.55	5.80
MICAL2	534041	3.39	3.45	7.05
TPM4	535277	2.63	1.66	2.56
MARCKSL1	539555	2.19	2.84	1.95
RAI14	525869	1.89	2.24	2.24
MYO18A	519634	−1.98	−1.51	−1.61
TNS3	516555	−3.31	−3.03	−3.13
Post-translational modification				
UFM1	530547	2.63	1.72	1.92
DPH3	511579	2.62	1.84	1.57
RWDD3	614557	−1.62	−2.22	−2.16
KBTBD4	617482	−1.74	−1.52	−1.59
TRIM68	538657	−2.30	−1.64	−1.54
Membrane transporter				
TRPC4	282102	4.33	3.33	3.50
SLC39A8	508193	2.86	2.58	3.73
SLC20A2	518905	2.79	1.89	1.53
SLC2A1	282356	2.44	2.43	4.71
SLC12A2	286845	1.78	2.69	1.57
DNA regulation and repair				
RBBP8	512977	4.08	1.99	3.10
H2AFZ	287016	1.61	1.54	1.55
PAPD7	523016	1.50	1.86	3.36
ZRANB3	529922	−1.88	−1.82	−1.53
MUM1	513471	−2.16	−1.71	−1.55
G-protein coupled receptor				
F2RL2	512581	2.17	1.82	3.34
AGTR1	281607	−2.16	−2.07	−1.95
APLNR	615435	−4.20	−2.76	−1.83
Chaperone				
DNAJA1	528862	2.31	1.60	1.51
HSPA2	281827	−1.96	−1.65	−1.57
Unknown				
C23H6orf141	100271839	2.45	1.98	6.27
LHFPL2	616131	2.35	3.32	2.16
LOC540312	540312	−1.81	−1.84	−4.54
CYYR1	768230	−1.98	−1.51	−2.08
LOC511229	511229	−2.33	−2.08	−1.77

representation of components of the IL-33 receptor complex (Romereim et al., 2017; Talbott et al., 2017). In the regressing CL, IL-33 could play a role in macrophage recruitment (Carlock et al.,

2014; Wu et al., 2015) and mast cell activation (Lott et al., 2015); and is likely derived from the endothelial cells rather than the steroidogenic cells of the CL (Carlock et al., 2014).

Another novel cytokine highlighted in this dataset is IL-17A, which is identified as an activated upstream regulator in three of the times examined. There are no reports of a role for IL-17 in the CL, however, a recent study by Ozkan et al. demonstrated that elevated serum IL-17 concentrations predicted infertility and poor responsiveness to *in vitro* fertilization (Ozkan et al., 2014). Analysis of this dataset using a more robust method of calling differentially expressed transcripts increased z-score predicted activation of IL-17 signaling (Yu et al., 2015), and our data indicate that IL-17 can directly activate NF-κB and ERK1/2 signaling in luteal cell cultures. How IL-33 and IL-17 contribute to luteal regression will be a subject of future investigations.

Cytokine signaling intermediates such as NF-κB and STAT3 are predicted by IPA to be activated in response to PGF2α throughout the time-course. Activation of NF-κB or prediction of NF-κB activation is consistently reported after PGF2α treatment *in vivo* (Mondal et al., 2011; Shah et al., 2014). However, *in vitro* PGF2α does not phosphorylate NF-κB in luteal cells (present study) or endometrial adenocarcinoma cells (Sales et al., 2009). Thus, *in vivo* PGF2α may use secondary mediators, such as cytokines, which would activate NF-κB and STAT signaling. Of interest, IPA also predicts the inhibition of SOCS1 and SOCS3 during the PGF2α time-course. This prediction is supported by significant increases in expression of SOCS3 transcripts within 1 h (4-fold) and SOCS1 at 4 h (1.7-fold), findings consistent with a well-controlled tissue-specific inflammatory response. This expands on work by ourselves and others that previously proposed a role for cytokines and immune cells in PGF2α-induced luteolysis after PGF2α treatment (Mondal et al., 2011; Shah et al., 2014; Shirasuna et al., 2012b; Talbott et al., 2014).

We found both direct and indirect evidence for increases in expression of pro-inflammatory cytokines and signaling during the early responses to PGF2α. Changes in cytokine-related transcripts do not occur until 2–4 h after PGF2α treatment; although, IPA predicts upstream cytokine activation and signaling at all 4 times examined. Secretion of cytokines (TNFα, TGFβ, and CXCL8) can be stimulated by PGF2α treatment in the ovary (Hou et al., 2008; Shaw and Britt, 1995), and other tissues (Sales et al., 2009). For example, PGF2α treatment *in vivo* and *in vitro* induces CXCL8, a chemokine which potentially serves to recruit neutrophils and macrophages to the CL (Atli et al., 2012; Shirasuna et al., 2012b; Talbott et al., 2014). The recruitment and activation of immune cells along with the actions of pre-formed cytokines could be responsible for the very early gene expression changes that are indicative of cytokine signaling. Both neutrophils and mast cells can store and release large amounts of cytokines and other bioactive proteins immediately after activation without the need for *de novo* synthesis of proteins (Sheshachalam et al., 2014; Wernersson and Pejler, 2014). This would allow for immediate responses without requiring transcription or translation; therefore, these genes would not be identified in transcriptome-based studies.

4.4. PGF2α activates well-organized signaling cascades

Analysis of SOMs demonstrates that a coordinated cascade of transcription occurs after PGF2α administration and includes immediate-early, early, delayed-early, late, and biphasic transcriptional responses. This suggests that a carefully orchestrated succession of gene expression changes occurs during PGF2α-induced luteolysis. As expected, the immediate-early upregulated and early downregulated responses are composed primarily of transcription factors. Later signaling waves contain a greater proportion of genes that are non-transcription factors suggesting that genes with an immediate-early expression profile could trigger transcription of early, and delayed-early type genes which could then alter transcription of late-type genes in a transcriptional cascade (Jothi et al., 2009).

Upregulated gene patterns are consistent with inflammatory response and activation of immune cells. The common upstream regulators TNFα, TGFβ, IL-1β, and NF-κB support this prediction. Downregulated SOMs correspond with the activation of death pathways and inhibition of cellular proliferation. Interestingly, upregulated SOMs had functional annotations such as decreased organismal death whereas downregulated SOMs noted increased organismal death, which highlights that during a complex event such as luteolysis, there are populations of cells, which are activated and proliferating (potentially immune cells), and other cell types that will be inhibited and primed for apoptosis such as endothelial and steroidogenic luteal cells. Notably, the common upstream regulators EDN1 and VEGF support the idea that luteal regression involves early changes in the vasculature, which has been previously suggested (Davis and Rueda, 2002). Moreover, several studies indicate that biphasic transcriptional responses are correlated with fluctuations in activation of NF-κB in response to cytokines like TNFα (Zambrano et al., 2016). These biphasic, oscillatory responses that can activate both acute and chronic changes within the target tissues are characteristic of cytokine and NF-κB signaling (Zambrano et al., 2016). In accordance, the cytokines IL-1β, and TNFα are predicted as upstream regulators of the upregulated biphasic response SOM. Additionally, Mondal et al., 2011 proposed that sustained activation of NF-κB signaling only occurred in PGF2α-sensitive luteal tissues, and the biphasic patterns of gene expression could reflect both acute activation and the beginning of a chronic activation of target genes. Together these SOMS indicate a cascade of events, whereby immediate-early response genes, composed mostly of transcription factors alters early and delayed-early gene expressions, which contribute to changes in the expression of late-response genes.

4.5. Dataset comparison and relationship to previous studies

Comparison of our dataset to two similar bovine luteal transcriptome studies, GSE23348 (Mondal et al., 2011) and GSE27961 (Shah et al., 2014) reveals 124 differentially expressed transcripts common to all three datasets, including *BCL6, BMP2*, *FOSL1, IL33, INHBA,* and *NR5A2*. Bioinformatics analysis of the common transcripts predicts activation of cytokine signaling and includes the upstream regulators IL-1β, TNFα, and TGFβ. This comparison provides several high confidence transcriptome changes that occur in the bovine CL after PGF2α treatment, which vary minimally across study sites and investigation groups, providing an important resource for future studies. Importantly, our analysis of the differentially expressed genes common to all three datasets as well as each independent dataset are consistent with the activation of both PGF2α and cytokine signaling. Additionally, functional annotations of common genes indicate a large proportion of gene products function in cytokine signaling and cell-cell interaction, which both play critical roles in luteolysis. These findings validate the predictions based on the short time-course and support a growing body of literature that suggests that immune cells and cytokines play a key role in luteal regression.

4.6. Conclusions from the study

Shortly after PGF2α administration, phospholipase C, PKC, Ca^{2+}, and ERK trigger a variety of signaling cascades to begin the luteolytic process. Our data suggests that *in vivo,* PGF2α administration

stimulates a series of transcriptional waves likely as a result of classical PGF2α and cytokine signaling events, as early as 30 min after PGF2α treatment. This is the beginning of a cascade of events that will initiate decreases in progesterone secretion (2–12 h after PGF2α) and result in the structural regression of the CL 12–18 h after PGF2α (Meidan, 2017; Yadav et al., 2002). The earliest decreases in progesterone secretion during luteolysis may be due to changes in transcriptional abundance of *LIPE*/HSL and other transcripts which regulate cholesterol availability rather than direct changes in the expression of mRNA encoding the primary steroidogenic enzymes. We propose that during the early stages of functional regression in combination with PGF2α, the reduction in progesterone, and increase in inflammatory cytokines (potentially including IL-33 and IL-17) contribute to luteal regression. As the intra-luteal concentrations of PGF2α and inflammatory cytokines increase they may act within an auto-amplification loop eventually reaching a critical point from which there is no rescue from the luteolytic cascade (Niswender et al., 2007). Future studies to identify the cell-specific transcriptional changes occurring in steroidogenic cells, endothelial cells, immune cells, and fibroblasts are needed to better understand the dynamic network of changes that enable functional and structural luteal regression.

Conference presentation

Heather Talbott, Xiaoying Hou, Babu Guda, John S. Davis. Pathway Analysis of temporal gene expression in the bovine corpus luteum following *in vivo* injection with prostaglandin F2α. Midwest Student Biomedical Research Forum, Creighton University, Omaha, NE. Feb. 18, 2012.

Funding

This work was supported by the Agriculture and Food Research Initiative from the USDA National Institute of Food and Agriculture (NIFA) [2014-67011-22280 Pre-doctoral award to HT, 2011-67015-20076 to JSD and ASC, and 2013-67015-20965 to ASC, JRW and JSD]; USDA Hatch grants [NEB26-202/W2112 to ASC, eNEB ANHL 26-213 to ASC and JRW, NEB 26-206 to ASC and JRW]; USDA Agricultural Research Service Project Plan [3040-31000-093-00D to RAC]; the VA Nebraska-Western Iowa Health Care System Department of Veterans Affairs, Office of Research and Development Biomedical Laboratory Research and Development funds (I01BX000512) [JSD]; and The Olson Center for Women's Health, Department of Obstetrics and Gynecology, Nebraska Medical Center, Omaha, NE [JSD]; National Institute for General Medical Science (NIGMS) [INBRE - P20GM103427-14, COBRE - 1P30GM110768-01 to University of Nebraska Microarray Core and the Bioinformatics and Systems Biology Core]; and The Fred & Pamela Buffett Cancer Center Support [P30CA036727 to University of Nebraska Microarray Core and the Bioinformatics and Systems Biology Core].

Additional footnotes

The U.S. Department of Agriculture (USDA) prohibits discrimination in all its programs and activities on the basis of race, color, national origin, age, disability, and where applicable, sex, marital status, familial status, parental status, religion, sexual orientation, genetic information, political beliefs, reprisal, or because all or part of an individual's income is derived from any public assistance program. (Not all prohibited bases apply to all programs.) Persons with disabilities who require alternative means for communication of program information (Braille, large print, audiotape, etc.) should contact USDA's TARGET Center at (202) 720–2600 (voice and TDD). To file a complaint of discrimination, write to USDA, Director, Office of Civil Rights, 1400 Independence Avenue, S.W., Washington, D.C. 20250-9410, or call (800) 795–3272 (voice) or (202) 720–6382 (TDD). USDA is an equal opportunity provider and employer.

This publication's contents are the sole responsibility of the authors and do not necessarily represent the official views of the NIH or NIGMS.

Acknowledgements

This work was supported by the University of Nebraska Microarray Core Facility and staff.

Appendix A. Supplementary data

Supplementary data related to this article can be found at http://dx.doi.org/10.1016/j.mce.2017.05.018.

References

Aboelenain, M., Kawahara, M., Balboula, A.Z., Montasser, A.E.-M., Zaabel, S.M., Okuda, K., Takahashi, M., 2015. Status of autophagy, lysosome activity and apoptosis during corpus luteum regression in cattle. J. Reprod. Dev. 61, 229–236. http://dx.doi.org/10.1262/jrd.2014-135.

Acosta, T.J., Yoshizawa, N., Ohtani, M., Miyamoto, A., 2002. Local changes in blood flow within the early and midcycle corpus luteum after prostaglandin F(2 alpha) injection in the cow. Biol. Reprod. 66, 651–658.

Arts, R.J.W., Joosten, L.A.B., van der Meer, J.W.M., Netea, M.G., 2013. TREM-1: intracellular signaling pathways and interaction with pattern recognition receptors. J. Leukoc. Biol. 93, 209–215. http://dx.doi.org/10.1189/jlb.0312145.

Arvisais, E., Hou, X., Wyatt, T.A., Shirasuna, K., Bollwein, H., Miyamoto, A., Hansen, T.R., Rueda, B.R., Davis, J.S., 2010. Prostaglandin F2alpha represses IGF-I-stimulated IRS1/phosphatidylinositol-3-kinase/AKT signaling in the corpus luteum: role of ERK and P70 ribosomal S6 kinase. Mol. Endocrinol. 24, 632–643. http://dx.doi.org/10.1210/me.2009-0312.

Atli, M.O., Bender, R.W., Mehta, V., Bastos, M.R., Luo, W., Vezina, C.M., Wiltbank, M.C., 2012. Patterns of gene expression in the bovine corpus luteum following repeated intrauterine infusions of low doses of prostaglandin F2alpha. Biol. Reprod. 86, 130. http://dx.doi.org/10.1095/biolreprod.111.094870.

Best, C.L., Pudney, J., Welch, W.R., Burger, N., Hill, J.A., 1996. Localization and characterization of white blood cell populations within the human ovary throughout the menstrual cycle and menopause. Hum. Reprod. 11, 790–797.

Bogan, R.L., Hennebold, J.D., 2010. The reverse cholesterol transport system as a potential mediator of luteolysis in the primate corpus luteum. Reproduction 139, 163–176. http://dx.doi.org/10.1530/REP-09-0005.

Carlock, C.I., Wu, J., Zhou, C., Tatum, K., Adams, H.P., Tan, F., Lou, Y., 2014. Unique temporal and spatial expression patterns of IL-33 in ovaries during ovulation and estrous cycle are associated with ovarian tissue homeostasis. J. Immunol. 193, 161–169. http://dx.doi.org/10.4049/jimmunol.1400381.

Chen, D.B., Westfall, S.D., Fong, H.W., Roberson, M.S., Davis, J.S., 1998. Prostaglandin F2alpha stimulates the Raf/MEK1/mitogen-activated protein kinase signaling cascade in bovine luteal cells. Endocrinology 139, 3876–3885. http://dx.doi.org/10.1210/endo.139.9.6197.

Chen, D., Fong, H.W., Davis, J.S., 2001. Induction of c-fos and c-jun messenger ribonucleic acid expression by prostaglandin F2alpha is mediated by a protein kinase C-dependent extracellular signal-regulated kinase mitogen-activated protein kinase pathway in bovine luteal cells. Endocrinology 142, 887–895. http://dx.doi.org/10.1210/endo.142.2.7938.

Davis, J.S., Rueda, B.R., 2002. The corpus luteum: an ovarian structure with maternal instincts and suicidal tendencies. Front. Biosci. 7, d1949–d1978.

Davis, J.S., Weakland, L.L., Weiland, D.A., Farese, R.V., West, L.A., 1987. Prostaglandin F2 alpha stimulates phosphatidylinositol 4,5-bisphosphate hydrolysis and mobilizes intracellular Ca2+ in bovine luteal cells. Proc. Natl. Acad. Sci. U. S. A. 84, 3728–3732.

Del Canto, F., Sierralta, W., Kohen, P., Muñoz, A., Strauss, J.F., Devoto, L., 2007. Features of natural and gonadotropin-releasing hormone antagonist-induced corpus luteum regression and effects of in vivo human chorionic gonadotropin. J. Clin. Endocrinol. Metab. 92, 4436–4443. http://dx.doi.org/10.1210/jc.2007-0125.

Gentleman, R.C., Carey, V.J., Bates, D.M., Bolstad, B., Dettling, M., Dudoit, S., Ellis, B., Gautier, L., Ge, Y., Gentry, J., Hornik, K., Hothorn, T., Huber, W., Iacus, S., Irizarry, R., Leisch, F., Li, C., Maechler, M., Rossini, A.J., Sawitzki, G., Smith, C., Smyth, G., Tierney, L., Yang, J.Y.H., Zhang, J., 2004. Bioconductor: open software development for computational biology and bioinformatics. Genome Biol. 5 http://dx.doi.org/10.1186/gb-2004-5-10-r80. R80.

Hou, X., Arvisais, E.W., Jiang, C., Chen, D., Roy, S.K., Pate, J.L., Hansen, T.R., Rueda, B.R., Davis, J.S., 2008. Prostaglandin F2alpha stimulates the expression and secretion of transforming growth factor B1 via induction of the early growth response 1 gene (EGR1) in the bovine corpus luteum. Mol. Endocrinol. 22, 403–414. http://

dx.doi.org/10.1210/me.2007-0272.
Huang, D.W., Sherman, B.T., Lempicki, R.A., 2009a. Bioinformatics enrichment tools: paths toward the comprehensive functional analysis of large gene lists. Nucleic Acids Res. 37, 1–13. http://dx.doi.org/10.1093/nar/gkn923.
Huang, D.W., Sherman, B.T., Lempicki, R.A., 2009b. Systematic and integrative analysis of large gene lists using DAVID bioinformatics resources. Nat. Protoc. 4, 44–57. http://dx.doi.org/10.1038/nprot.2008.211.
Jothi, R., Balaji, S., Wuster, A., Grochow, J.A., Gsponer, J., Przytycka, T.M., Aravind, L., Babu, M.M., 2009. Genomic analysis reveals a tight link between transcription factor dynamics and regulatory network architecture. Mol. Syst. Biol. 5 http://dx.doi.org/10.1038/msb.2009.52, 294.
Kurusu, S., Iwao, M., Kawaminami, M., Hashimoto, I., 1998. Involvement of cytosolic phospholipase A2 in the ovulatory process in gonadotropin-primed immature rats. Prostagl. Leukot. Essent. Fat. Acids 58, 405–411.
Kurusu, S., Sapirstein, A., Bonventre, J.V., 2012. Group IVA phospholipase A2 optimizes ovulation and fertilization in rodents through induction of and metabolic coupling with prostaglandin endoperoxide synthase 2. FASEB J. 26, 3800–3810. http://dx.doi.org/10.1096/fj.12-203968.
Levy, N., Kobayashi, S., Roth, Z., Wolfenson, D., Miyamoto, A., Meidan, R., 2000. Administration of prostaglandin f(2 alpha) during the early bovine luteal phase does not alter the expression of ET-1 and of its type A receptor: a possible cause for corpus luteum refractoriness. Biol. Reprod. 63, 377–382.
Lott, J.M., Sumpter, T.L., Turnquist, H.R., 2015. New dog and new tricks: evolving roles for IL-33 in type 2 immunity. J. Leukoc. Biol. 97, 1037–1048. http://dx.doi.org/10.1189/jlb.3RI1214-595R.
Lund, E.G., Kerr, T.A., Sakai, J., Li, W.P., Russell, D.W., 1998. cDNA cloning of mouse and human cholesterol 25-hydroxylases, polytopic membrane proteins that synthesize a potent oxysterol regulator of lipid metabolism. J. Biol. Chem. 273, 34316–34327.
Manna, P.R., Cohen-Tannoudji, J., Counis, R., Garner, C.W., Huhtaniemi, I., Kraemer, F.B., Stocco, D.M., 2013. Mechanisms of action of hormone-sensitive lipase in mouse Leydig cells: its role in the regulation of the steroidogenic acute regulatory protein. J. Biol. Chem. 288, 8505–8518. http://dx.doi.org/10.1074/jbc.M112.417873.
Mao, D., Hou, X., Talbott, H.A., Cushman, R., Cupp, A., Davis, J.S., 2013. ATF3 expression in the corpus luteum: possible role in luteal regression. Mol. Endocrinol. 27, 2066–2079. http://dx.doi.org/10.1210/me.2013-1274.
Maroni, D., Davis, J.S., 2011. TGFB1 disrupts the angiogenic potential of microvascular endothelial cells of the corpus luteum. J. Cell Sci. 124, 2501–2510. http://dx.doi.org/10.1242/jcs.084558.
Maroni, D., Davis, J.S., 2012. Transforming growth factor beta 1 stimulates profibrotic activities of luteal fibroblasts in cows. Biol. Reprod. 87, 1–11. http://dx.doi.org/10.1095/biolreprod.112.100735.
McCann, T.J., Flint, A.P., 1993. Use of pertussis toxin to investigate the mechanism of action of prostaglandin F2 alpha on the corpus luteum in sheep. J. Mol. Endocrinol. 10, 79–85.
Meidan, R. (Ed.), 2017. The Life Cycle of the Corpus Luteum. Springer International Publishing, Cham. http://dx.doi.org/10.1007/978-3-319-43238-0.
Mi, H., Muruganujan, A., Casagrande, J.T., Thomas, P.D., 2013. Large-scale gene function analysis with the PANTHER classification system. Nat. Protoc. 8, 1551–1566. http://dx.doi.org/10.1038/nprot.2013.092.
Mi, H., Poudel, S., Muruganujan, A., Casagrande, J.T., Thomas, P.D., 2016. PANTHER version 10: expanded protein families and functions, and analysis tools. Nucleic Acids Res. 44, D336–D342. http://dx.doi.org/10.1093/nar/gkv1194.
Micks, E., Raglan, G.B., Schulkin, J., 2015. Bridging progestogens in pregnancy and pregnancy prevention. Endocr. Connect. 4, R81–R92. http://dx.doi.org/10.1530/EC-15-0093.
Mondal, M., Schilling, B., Folger, J., Steibel, J.P., Buchnick, H., Zalman, Y., Ireland, J.J., Meidan, R., Smith, G.W., 2011. Deciphering the luteal transcriptome: potential mechanisms mediating stage-specific luteolytic response of the corpus luteum to prostaglandin $F_2\alpha$. Physiol. Genomics 43, 447–456. http://dx.doi.org/10.1152/physiolgenomics.00155.2010.
Nishimura, R., Okuda, K., 2015. Multiple roles of hypoxia in ovarian function: roles of hypoxia-inducible factor-related and -unrelated signals during the luteal phase. Reprod. Fertil. Dev. http://dx.doi.org/10.1071/RD15010.
Niswender, G.D., Davis, T.L., Griffith, R.J., Bogan, R.L., Monser, K., Bott, R.C., Bruemmer, J.E., Nett, T.M., 2007. Judge, jury and executioner: the autoregulation of luteal function. Soc. Reprod. Fertil. Suppl. 64, 191–206.
Ozkan, Z.S., Deveci, D., Kumbak, B., Simsek, M., Ilhan, F., Sekercioglu, S., Sapmaz, E., 2014. What is the impact of Th1/Th2 ratio, SOCS3, IL17, and IL35 levels in unexplained infertility? J. Reprod. Immunol. 103, 53–58. http://dx.doi.org/10.1016/j.jri.2013.11.002.
O'Shaughnessy, P.J., Wathes, D.C., 1985. Role of lipoproteins and de-novo cholesterol synthesis in progesterone production by cultured bovine luteal cells. Reproduction 74, 425–432. http://dx.doi.org/10.1530/jrf.0.0740425.
Pate, J.L., Toyokawa, K., Walusimbi, S., Brzezicka, E., 2010. The interface of the immune and reproductive systems in the ovary: lessons learned from the corpus luteum of domestic animal models. Am. J. Reprod. Immunol. 64, 275–286. http://dx.doi.org/10.1111/j.1600-0897.2010.00906.x.
Penny, L.A., Armstrong, D.G., Baxter, G., Hogg, C., Kindahl, H., Bramley, T.A., Watson, E.D., Webb, R., 1998. Expression of monocyte chemoattractant protein-1 in the bovine corpus luteum around the time of natural luteolysis. Biol. Reprod. 59, 1464–1469.
Penny, L.A., Armstrong, D., Bramley, T.A., Webb, R., Collins, R.A., Watson, E.D., 1999. Immune cells and cytokine production in the bovine corpus luteum throughout the oestrous cycle and after induced luteolysis. J. Reprod. Fertil. 115, 87–96. http://dx.doi.org/10.1530/jrf.0.1150087.
R Core Team, 2015. R: A Language and Environment for Statistical Computing.
Romereim, S.M., Summers, A.F., Pohlmeier, W.E., Zhang, P., Hou, X., Talbott, H.A., Cushman, R.A., Wood, J.R., Davis, J.S., Cupp, A.S., 2017. Gene expression profiling of bovine ovarian follicular and luteal cells provides insight into cellular identities and functions. Mol. Cell. Endocrinol. 439, 379–394. http://dx.doi.org/10.1016/j.mce.2016.09.029.
Sales, K.J., Maldonado-Pérez, D., Grant, V., Catalano, R.D., Wilson, M.R., Brown, P., Williams, A.R.W., Anderson, R.A., Thompson, E.A., Jabbour, H.N., 2009. Prostaglandin F(2alpha)-F-prostanoid receptor regulates CXCL8 expression in endometrial adenocarcinoma cells via the calcium-calcineurin-NFAT pathway. Biochim. Biophys. Acta 1793, 1917–1928. http://dx.doi.org/10.1016/j.bbamcr.2009.09.018.
Salverson, R.R., DeJarnette, J.M., Marshall, C.E., Wallace, R.A., 2002. Synchronization of estrus in virgin beef heifers using melengestrol acetate and PGF2alpha: an efficacy comparison of cloprostenol and dinoprost tromethamine. Theriogenology 57, 853–858.
Schaper, F., Rose-John, S., 2015. Interleukin-6: biology, signaling and strategies of blockade. Cytokine Growth Factor Rev. 26, 475–487. http://dx.doi.org/10.1016/j.cytogfr.2015.07.004.
Seto, N.L., Bogan, R.L., 2015. Decreased cholesterol uptake and increased liver x receptor-mediated cholesterol efflux pathways during prostaglandin F2 alpha-induced and spontaneous luteolysis in sheep. Biol. Reprod. 92 http://dx.doi.org/10.1095/biolreprod.114.124941, 128.
Shah, K.B., Tripathy, S., Suganthi, H., Rudraiah, M., 2014. Profiling of luteal transcriptome during prostaglandin F2-alpha treatment in buffalo cows: analysis of signaling pathways associated with luteolysis. PLoS One 9. http://dx.doi.org/10.1371/journal.pone.0104127 e104127.
Shaw, D.W., Britt, J.H., 1995. Concentrations of tumor necrosis factor alpha and progesterone within the bovine corpus luteum sampled by continuous-flow microdialysis during luteolysis in vivo. Biol. Reprod. 53, 847–854.
Sheshachalam, A., Srivastava, N., Mitchell, T., Lacy, P., Eitzen, G., 2014. Granule protein processing and regulated secretion in neutrophils. Front. Immunol. 5 http://dx.doi.org/10.3389/fimmu.2014.00448, 448.
Shirasuna, K., 2010. Nitric oxide and luteal blood flow in the luteolytic cascade in the cow. J. Reprod. Dev. 56, 9–14.
Shirasuna, K., Sasahara, K., Matsui, M., Shimizu, T., Miyamoto, A., 2010. Prostaglandin F2alpha differentially affects mRNA expression relating to angiogenesis, vasoactivation and prostaglandins in the early and mid corpus luteum in the cow. J. Reprod. Dev. 56, 428–436.
Shirasuna, K., Akabane, Y., Beindorff, N., Nagai, K., Sasaki, M., Shimizu, T., Bollwein, H., Meidan, R., Miyamoto, A., 2012a. Expression of prostaglandin $F2\alpha$ ($PGF2\alpha$) receptor and its isoforms in the bovine corpus luteum during the estrous cycle and $PGF2\alpha$-induced luteolysis. Domest. Anim. Endocrinol. 43, 227–238. http://dx.doi.org/10.1016/j.domaniend.2012.03.003.
Shirasuna, K., Jiemtaweeboon, S., Raddatz, S., Nitta, A., Schuberth, H.-J., Bollwein, H., Shimizu, T., Miyamoto, A., 2012b. Rapid accumulation of polymorphonuclear neutrophils in the corpus luteum during prostaglandin $F(2\alpha)$-induced luteolysis in the cow. PLoS One 7. http://dx.doi.org/10.1371/journal.pone.0029054 e29054.
Sirinian, M.I., Belleudi, F., Campagna, F., Ceridono, M., Garofalo, T., Quagliarini, F., Verna, R., Calandra, S., Bertolini, S., Sorice, M., Torrisi, M.R., Arca, M., 2005. Adaptor protein ARH is recruited to the plasma membrane by low density lipoprotein (LDL) binding and modulates endocytosis of the LDL/LDL receptor complex in hepatocytes. J. Biol. Chem. 280, 38416–38423. http://dx.doi.org/10.1074/jbc.M504343200.
Smyth, G.K., 2004. Linear models and empirical bayes methods for assessing differential expression in microarray experiments. Stat. Appl. Genet. Mol. Biol. 3 http://dx.doi.org/10.2202/1544-6115.1027. Article3.
Spencer, T.E., Forde, N., Lonergan, P., 2016. The role of progesterone and conceptus-derived factors in uterine biology during early pregnancy in ruminants. J. Dairy Sci. 99, 5941–5950. http://dx.doi.org/10.3168/jds.2015-10070.
Summers, A.F., Pohlmeier, W.E., Sargent, K.M., Cole, B.D., Vinton, R.J., Kurz, S.G., McFee, R.M., Cushman, R.A., Cupp, A.S., Wood, J.R., 2014. Altered theca and cumulus oocyte complex gene expression, follicular arrest and reduced fertility in cows with dominant follicle follicular fluid androgen excess. PLoS One 9. http://dx.doi.org/10.1371/journal.pone.0110683 e110683.
Sun, L.-P., Li, L., Goldstein, J.L., Brown, M.S., 2005. Insig required for sterol-mediated inhibition of Scap/SREBP binding to COPII proteins in vitro. J. Biol. Chem. 280, 26483–26490. http://dx.doi.org/10.1074/jbc.M504041200.
Szklarczyk, D., Franceschini, A., Wyder, S., Forslund, K., Heller, D., Huerta-Cepas, J., Simonovic, M., Roth, A., Santos, A., Tsafou, K.P., Kuhn, M., Bork, P., Jensen, L.J., von Mering, C., 2015. STRING v10: protein-protein interaction networks, integrated over the tree of life. Nucleic Acids Res. 43, D447–D452. http://dx.doi.org/10.1093/nar/gku1003.
Talbott, H.A., Delaney, A., Zhang, P., Yu, Y., Cushman, R.A., Cupp, A.S., Hou, X., Davis, J.S., 2014. Effects of IL8 and immune cells on the regulation of luteal progesterone secretion. Reproduction 148, 21–31. http://dx.doi.org/10.1530/REP-13-0602.
Talbott, H.A., Hou, X., Qiu, F., Guda, C., Yu, F., Cushman, R.A., Wood, J.R., Wang, C., Cupp, A.S., Davis, J.S., 2017. Transcriptomic and bioinformatic analysis of short prostaglandin F2 alpha time-course in bovine corpus luteum. Data Br. (in press).
Tamayo, P., Slonim, D., Mesirov, J., Zhu, Q., Kitareewan, S., Dmitrovsky, E., Lander, E.S., Golub, T.R., 1999. Interpreting patterns of gene expression with self-organizing maps: methods and application to hematopoietic

differentiation. Proc. Natl. Acad. Sci. U. S. A. 96, 2907–2912.
Thomas, P.D., Kejariwal, A., Guo, N., Mi, H., Campbell, M.J., Muruganujan, A., Lazareva-Ulitsky, B., 2006. Applications for protein sequence-function evolution data: mRNA/protein expression analysis and coding SNP scoring tools. Nucleic Acids Res. 34, W645–W650.
Toaff, M.E., Schleyer, H., Strauss, J.F., 1982. Metabolism of 25-hydroxycholesterol by rat luteal mitochondria and dispersed cells. Endocrinology 111, 1785–1790. http://dx.doi.org/10.1210/endo-111-6-1785.
Townson, D.H., Liptak, A.R., 2003. Chemokines in the corpus luteum: implications of leukocyte chemotaxis. Reprod. Biol. Endocrinol. 1 http://dx.doi.org/10.1186/1477-7827-1-94, 94.
Väänänen, J.E., Lee, S., Väänänen, C.C., Yuen, B.H., Leung, P.C., 1998. Stepwise activation of the gonadotropic signal transduction pathway, and the ability of prostaglandin F2alpha to inhibit this activated pathway. Endocrine 8, 301–307.
Wernersson, S., Pejler, G., 2014. Mast cell secretory granules: armed for battle. Nat. Rev. Immunol. 14, 478–494. http://dx.doi.org/10.1038/nri3690.
Wu, J., Carlock, C., Zhou, C., Nakae, S., Hicks, J., Adams, H.P., Lou, Y., 2015. IL-33 is required for disposal of unnecessary cells during ovarian atresia through regulation of autophagy and macrophage migration. J. Immunol. 194, 2140–2147. http://dx.doi.org/10.4049/jimmunol.1402503.
Yadav, V.K., Medhamurthy, R., 2006. Dynamic changes in mitogen-activated protein kinase (MAPK) activities in the corpus luteum of the bonnet monkey (Macaca radiata) during development, induced luteolysis, and simulated early pregnancy: a role for p38 MAPK in the regulation of luteal functio. Endocrinology 147, 2018–2027. http://dx.doi.org/10.1210/en.2005-1372.
Yadav, V.K., Sudhagar, R.R., Medhamurthy, R., 2002. Apoptosis during spontaneous and prostaglandin F(2alpha)-induced luteal regression in the buffalo cow (Bubalus bubalis): involvement of mitogen-activated protein kinases. Biol. Reprod. 67, 752–759. http://dx.doi.org/10.1095/biolreprod.102.004077.
Youngquist, R.S., Garverick, H.A., Keisler, D.H., 1995. Use of umbilical cord clamps for ovariectomy in cows. J. Am. Vet. Med. Assoc. 207, 474–475.
Yu, F., Chen, M.-H.M.-H., Kuo, L., Talbott, H.A., Davis, J.S.J.S., 2015. Confident difference criterion: a new Bayesian differentially expressed gene selection algorithm with applications. BMC Bioinforma. 16 http://dx.doi.org/10.1186/s12859-015-0664-3, 245.
Zambrano, S., De Toma, I., Piffer, A., Bianchi, M.E., Agresti, A., 2016. NF-κB oscillations translate into functionally related patterns of gene expression. Elife 5. http://dx.doi.org/10.7554/eLife.09100 e09100.